

A Study of Melt Ratio and Microstructure in Dissimilar Fusion Welds

Parchuri Pradeep Kumar

A Dissertation Submitted to
Indian Institute of Technology Hyderabad
In Partial Fulfillment of the Requirements for
The Degree of Master of Technology/ Doctor of Philosophy



भारतीय प्रौद्योगिकी संस्थान हैदराबाद
Indian Institute of Technology Hyderabad

Department of Materials Science and Metallurgical Engineering

July, 2016

Declaration

I declare that this written submission represents my ideas in my own words, and where others' ideas or words have been included, I have adequately cited and referenced the original sources. I also declare that I have adhered to all principles of academic honesty and integrity and have not misrepresented or fabricated or falsified any idea/data/fact/source in my submission. I understand that any violation of the above will be a cause for disciplinary action by the Institute and can also evoke penal action from the sources that have thus not been properly cited, or from whom proper permission has not been taken when needed.

A handwritten signature in blue ink that reads "P. Pradeep Kumar". The signature is written in a cursive style and is positioned above a horizontal line.

(Signature)

Parchuri Pradeep Kumar


MS14MTECH11004

Approval Sheet

This thesis entitled “A study of Melt Ratio and Microstructure in Dissimilar Fusion Welds” by Parchuri Pradeep Kumar is approved for the degree of Master of Technology from IIT Hyderabad.



Dr. Saswata Bhattacharya
Department of Materials Science and Metallurgical Engineering
Examiner



Dr. Atul Suresh Deshpande
Department of Materials Science and Metallurgical Engineering
Examiner



Dr. Subhradeep Chatterjee
Department of Materials Science and Metallurgical Engineering
Adviser



Dr. Chinthapenta R Viswanath
Department of Mechanical and Aerospace Engineering
Chairman

Acknowledgements

I humbly prostrate myself before the Almighty for his grace and abundant blessings which enabled me to complete this work successfully.

It gives me an immense pleasure to express my deepest sense of gratitude to my supervisors Dr. Subhradeep Chatterjee and Dr. Viswanath Chinthapenta for their invaluable guidance, motivation constant inspiration and co-operation that enabled me in bringing up this report in present elegant form. I am out of words to thank them. I feel very lucky to get them as my supervisors.

I am extremely thankful to Dr. Zaid Ahmed, Mr. Soumya Bandyopadhyay, Mr. Brijesh, Mr. Vinayak, Mr. Seelam, Mr. Bharathi, Mr. Soumen, Mr. Tamboli and Mr. Sreenivas K, Scholars who have helped and motivated me a lot to complete our work. I thank Dr. Saswatha Bhattacharya, faculty at Department of MSME, IIT Hyderabad for being inspirational to me throughout my Masters.

I cherish to acknowledge the benevolence of my parents. Lastly I sincerely thank to all of those who have directly or indirectly helped for the work reported here in.

Dedicated to

To my Parents, who are the reason for who I am now!

Abstract

Joining of dissimilar metals, which offers many engineering applications, is a challenge since 1950s. We need to produce the joint possess mechanical properties that matches the real time applications. Mechanical properties depend on the microstructural features. The microstructural features depend on local prevailing conditions during solidification and post-solidification cooling.

We studied the microstructure in the Ti/Ni laser welds using optical microscope, scanning electron microscope (SEM) and X-ray diffraction (XRD). The welds are asymmetric with respect to the initial butt joint. Despite its higher melting point, Ti melts more than Ni due to its lower thermal conductivity, but because of the high density of Ni the average composition of the weld is Ti–50at%Ni. Composition changes very steeply near the fusion interfaces in both Ti and Ni with associated microstructural changes. The variation is of much lesser magnitude in the rest of the weld, reflecting a well-mixed melt pool on a macroscopic scale. Growth of base metal grains into the weld pool at the fusion interfaces were found to be severely restricted at both Ti and Ni ends. The Ti fusion interface is marked by a band consisting of Ti_2Ni dendrites which grow toward the Ti base metal and stopped base metal grains into weld pool. Layers of intermetallic phases (Ni_3Ti , $Ni_3Ti+TiNi$, $TiNi$) form at the Ni fusion interface. $TiNi$ and Ti_2Ni are the major phases that appear in the bulk of the weld. From XRD results show that solid state transformation of $TiNi$ leads to the formation of the R-phase and martensite, which reflect the composition heterogeneity in the weld. Non-equilibrium phase Ni_2Ti was also observed in the weld.

Welding processing parameters (heat input, welding speed and thickness) and thermal properties of materials are important in deciding the extent of base metal melting and cooling rate which governs the microstructural features. We attempted to calculate melt ratios of dissimilar metal welds by solving heat conduction equation through ANSYS APDL, for different combinations of dissimilar couple. Then we estimated the average weld composition for Cu/Ni and Ti/Ni dissimilar couple for a given processing parameters

Contents

List of Figures	ix
List of Tables	x
1 Introduction	1
1.1 Similar metal welding VS Dissimilar metal welding.....	1
2 Literature Review	5
2.1 Classification.....	5
2.1.1 Gas welding.....	5
2.1.2 Arc welding.....	5
2.1.3 High energy beam welding.....	8
2.1.4 Non-fusion welding process.....	
2.2 Processing Parameters.....	9
2.2.1 Current.....	9
2.2.2 Travel speed of welding torch.....	10
2.3 Effect of welding parameters on weld pool shape.....	10
2.4 Heat flow in welds.....	12
2.4.1 Rosenthal's heat flow model.....	12
2.4.2 Goldak heat source.....	13
2.5 Motivation for the present work.....	13
2.6 Conclusions from literature review.....	16
2.7 Objective.....	17
3 Experimental Procedure	17
3.1 Laser welded sample processing conditions.....	17
3.2 Equipment used.....	17
3.3 Experimental steps involved.....	18
3.4 Computational details.....	19
3.5 Algorithm for solving heat conduction equation through ANSYS APDL...	19
3.6 Computational data.....	21
4 Results and Discussions	23

4.1 Average weld composition.....	23
4.2 XRD analysis.....	25
4.3 Microstructural analysis.....	27
4.3.1 Ti interface.....	27
4.3.2 Ni interface.....	29
4.3.3 Middle of the weld pool.....	31
4.3.4 Bottom of the weld pool.....	32
4.4 Computational Study.....	34
4.4.1 Rosenthal’s analytical model.....	34
4.4.2 Finite element method.....	35
4.5 Average weld composition in dissimilar couple.....	38
4.5.1 Cu/Ni joint.....	38
5 Summary	42
References.....	44

List of figures

2.1 Polarities in GTAW (from [1])	7
2.2 a) Globular Transfer b) Spray Transfer (from [2]).....	7
2.3 a) effect of thermal conductivity of a base metal on weld pool and surrounded HAZ b) effect of speed of welding on weld pool and surrounded weld pool. (from [1])	11
2.4 Two-dimensional heat flow during welding of thick work piece. (from [2]).....	12
3.1 a) Manual paper polishing machine. (b) Manual cloth polishing machine.....	17
3.2 a) Optical Microscopy (b) Scanning electron microscopy.....	18
3.3 Flow chart of algorithm used.....	20
3.4 Butt joint configuration, boundary conditions applied.....	22
4.1 Phase diagram of Ti/Ni binary couple (from [35])	24
4.2 Asymmetric weld pool with compositional variation	24
4.3 plot between Intensity VS 2θ	26
4.4 M_s , temperature variation with respect to Nickel content.....	26
4.5 a) Ti interface at low magnification (b, c) at higher magnification of Fig. (a), which shows Ti_2Ni dendrites growing towards the Ti base metal interface.....	28
4.6 (1, 2, and 3): Three zones at Ni interface.....	30
4.7 TiNi dendrites growing in both directions.....	31
4.8 Middle of the weld pool. a) Fine and coarse bands of TiNi b) Impurities of TiN on TiNi dendrites.....	32
4.9 a) bottom of the weld pool, (b, c, d, e) magnified different portions of Fig (a).	33
4.10 Block of TiNi dendrites segregated at the bottom of the weld pool.....	33
4.11 At% Ti variation with heat input (J/m).....	34
4.12 Symmetric temperature contours about the interface.....	36
4.13 1K rise in temperature by applying heat flux of $1J/m^2$	37
4.14 Plot between the maximum temperatures reached in each of the load step versus the time.....	38
4.15 Temperature contours evolution in Cu/Ni joint	40

List of tables

3.1 Laser welded sample processing conditions.....	17
3.2 Material thermal property data for Copper (from [34])	21
3.3 Material property data for Nickel (from [34])	21
3.4 Processing parameters used in modelling	21

Chapter 1

Introduction

Welding is the process of making two parts into one by accomplishing bonds between them with the help of heat and pressure. There are two classifications in welding processes: Fusion welding and Non-fusion welding. The details about these can be found in many standard books [1, 2]. When a significant amount of melting is involved in the process it is called fusion welding processes. For fusion welding processes the bond will be accomplished by melting and providing a supply of highly mobile atoms throughout the interface. Examples: Gas-metal arc welding (GMAW), Submerged arc welding (SAW), Gas-tungsten arc welding (GTAW) etc. Fusion welding processes are the most preferred over Non-fusion welding process because of the advantages: good metallurgical bonds and mechanical integrity [3].

Modern engineering designs demand: high specific strength, heat resistance, fatigue load resistance, toughness and corrosion resistance etc. To get a material possess all these properties is impossible. Joining two materials to get the combined properties from both of them to satisfy the design requirements is a choice available for us to this problem. Now dissimilar metal joining has become the most attractive field of research for manufacturers. The focus is on, establishing a suitable process and processing variables to join dissimilar metals to get the required mechanical properties.

1.1 Similar metal welding VS Dissimilar metal welding

Similar metal welding characteristic features are: (i) Symmetry in the weld pool shape, which is the result of both the base plates have thermo-physical properties same. This helps both the base plates to melt equal amounts. (ii) Epitaxial growth, rather than nucleating a new phase.

Distinctive features of dissimilar metal joints include: (i) Asymmetry in the weld pool shape because of the thermo-physical property variation between both the base materials. Both materials cannot melt equal amounts, which results into asymmetry in the weld pool. (ii) Asymmetry in the solidification rate, the thermal properties of materials are different, which obviously make solidification rates also different in both the base materials. (iii) Density driven flow may dominate. The physical properties (especially density) of the base plates are different.

This difference in densities can drive the density driven flow. Moreover there is no thumb rule that resulting intermetallic compounds (IMCs) should have the same density as base materials, which may contribute to the density driven flow in the weld pool. (iv) Base metal grains may not grow into the weld pool. Lippold et al. [4] conducted experiments on ferritic stainless steel and pearlitic stainless steel as base metals and a facecentered-cubic (FCC) filler metal to characterize the nature and character of the elevated temperature fusion boundary to determine the nucleation and growth characteristics of dissimilar metal welds (DMWs). The base metal side not observed base metal grains into weld pool at ferritic stainless steel interface, whereas base metal grains grown into the weld pool at pearlitic stainless steel interface. Phanikumar et al. [5] observed base metal grains growing into the weld pool from both the interfaces in Cu/Ni dissimilar metal joint by laser welding. Chatterjee et al. [6] observed Ti₂Ni dendrites growing towards Ti base metal side from the weld pool. The reasons for these observations were composition gradient present at the interface.

The problems involved in dissimilar joining are: (i) Brittle IMCs formation, there is always a chance of formation of brittle intermetallic compounds. Since they are present in the phase diagram, it is unavoidable during solidification of welding. Presence of intermetallic compounds makes joint very brittle and can fail easily, which is very bad for applications. The first and basic study on Ti/Ni was done by Steresky and Ryba [7] by LW process. They observed, that the joint was very brittle because of IMCs formation. Ti₂Ni, TiNi and TiNi₃ brittle IMCs are readily produced with in the weld during Ti/Ni dissimilar fiber laser welding [8]. Nano-sized granular Ti₇Al₅Si₁₂, serrated-shaped TiAl₃ IMCs are observed in laser welding-brazing of 5A06-Ti-6Al-4V alloys [9]. A layer of IMCs: Ti₂Cu, TiCu and AlCu₂Ti present in titanium- weld interface, in Cu-Ti welded joints by cold metal transfer process [10]. Cu₄Ti, Cu₂Ti, Cu₃Ti₂, Cu₄Ti₃ and CuTi intermetallic phases were formed in the bonding interface of Ti6Al4V titanium alloy and electrolytic grade 99.99% copper using diffusion bonding [11]. Fe₂Al₅, FeAl₃ IMCs are observed at the interface of Fe in Fe/Al laser welding process [12]. TiAl, Ti₃Al IMCs were observed in Ti/Al joints of laser welding, depending on how much Al melted [13]. IMCs of Cu-Al (Al₂Cu, Al₄Cu₉, AlCu) are observed at the interfaces in Cu/Al GMAW; showed by using a proper filler can reduce the thickness of IMCs [14]. IMCs MgCu₂ and Mg₂Cu made the weld of Cu/Mg by GTAW, very weak [15]

(ii) Residual stresses. In similar and DMWs, residual stresses are generated by the thermal contraction of the weld metal and the adjacent heated parent metal, and hence the residual stress distribution in an as-welded DMW is broadly similar to that in a similar metal weld. If the structure containing the DMW is subject to post-weld heat treatment (PWHT), then its residual stresses will be completely different from those at similar metal welds. Most of the original as-welded residual stresses will be relieved during the heat-up and hold period of the PWHT procedure. During cool down, a new set of residual stresses will be generated because of the differential contractions of the different regions. These are very bad for mechanical properties, and are responsible for the initiation of cracks. Mai and Spowage [16] observed, within the weld pool the residual stress increased rapidly to highly tensile values in laser welding of steel-kovar joint.

(iii) Segregation. As base metals densities are different; there would be a problem of segregation of high density elements or compounds at the bottom of the weld pool, either as a single constituent or in the form of IMC. Chatterjee et al. [6] observed preferential occurrence of TiNi dendrites at the bottom of the weld pool in laser welded Ti/Ni binary couple. Huang, Kou observed severe amount of Cu segregation in occurred in the weld metal during solidification, which resulted poor microstructure and mechanical properties in gas metal arc welding of Aluminium alloy 2219. Segregation is a problem observed in both similar and dissimilar metal welds. In dissimilar metals welds density differences are may high that, segregation is always a problem. By overcoming all the difficulties and joining dissimilar joints by any fusion welding process is a challenge.

High-energy beam welding processes (Laser welding (LW), Electron beam welding (EB)) are quite impressive than all the other existing processes of fusion welding to join dissimilar metal joints by providing advantages: narrow fusion zone, the ability to precisely locate the weld, a favorable fusion zone form and high power density have proven to be of advantage for the welding of dissimilar metals [17]. Metzger and Lison [18] presented a feasibility study of electron beam welding on thirty three dissimilar binary couple, one ternary and one quinary combinations. Weld characterization was mostly by macroscopic examination (macroscopic cracks, weld appearance) and did not include any detailed microstructural studies. The advantages of LW process for dissimilar metal welding are covered in detail in [19].

Microstructure decides the mechanical properties of the joint. Fusion zone microstructure depends on the average weld composition. All the solidification reactions are the function of average weld composition. Average weld composition is the function of processing parameters [8] as well as thermo-physical properties of the materials.

We, in our work tried to understand the microstructural variation in Ti/Ni laser welded dissimilar couple with variation in velocity, which is one of the processing parameters. We are mostly concern about the average weld composition variation with processing parameters. We tried to explore it computationally by modelling Rosenthal analytical heat source model. And then we tried with the more accurate model than Rosenthal analytical model, which is finite element method (numerical model) to verify the primary result, which we observed in analytical modelling.

This thesis is organised as follows. We have given a brief literature review in Chapter 2. A detailed experimental procedure is presented in Chapter 3. We then presented the results of microstructural details of Ti/Ni LW joint in Chapter 4. We have showed the computational results of both analytical and numerical models in Chapter 4. Then we finish the thesis with summary from our study (Chapter 5).

Chapter 2

Literature Review

2.1 Classification

Welding can be broadly classified into two types: Fusion welding, Non-fusion welding.

The process in which base materials are melted, to make the weld called the fusion welding. There are three major types in this process: Gas welding, Arc welding, High-energy beam welding.

2.1.1 Gas welding

This is the process which makes use of different types of flames (Oxidizing, Reducing, Neutral), depending on the requirement and which is generated by a reaction between a fuel gas and oxygen to melt the base materials to join them. Oxy acetylene gas welding is the most familiar one, as it possess high flame temperature. Most appreciable thing about this process is the equipment is simple, portable, and inexpensive. The productivity, high amount of HAZ because of high heat input and limited protection power are the limitations of this process.

Neutral flame: It is the most commonly used flame for all the metals, which has equal amounts of C_2H_2 and O_2 .

Reducing flame: Uses excess acetylene for combustion. It mostly employed to weld aluminium alloys, as it oxidizes easily.

Oxidizing flame: A short whiter inner cone is the characteristic feature of oxidizing flame. This flame is preferred to weld brass because copper oxide covers the weld pool and prevents zinc evaporation.

2.1.2 Arc welding:

This is the process which establish an arc between the electrode and the base materials by the use of weld power supply to melt them and to create the joint. Variety of processes are available: Manual, automatic or semi-automatic.

Shielded metal arc welding (SMAW), Gas-metal arc welding, Gas-tungsten arc welding, Submerged arc welding etc. come under this category.

Shielded metal arc welding: An arc is established between the metal and stick like covered electrode to heat, melt and join the metal pieces. Often refers as stick welding. The electrode holder is connected through a welding cable to one terminal of the power source and the work piece is connected through a second cable to the other terminal of the power source. Covering of electrodes contain different chemicals meant for different functions: deoxidation, protection, arc stabilization, metal addition.

SMAW is employed for mostly maintenance, repair, and field construction as it is very inexpensive and simple. Not suitable for reactive metals as no gas employed to protect them.

Gas-tungsten arc welding: Arc is established between a non-consumable tungsten electrode and the metal to heat, melt and join the metal pieces. Protection from air is better in this process as helium or argon is used as shielding gases. Sometimes we can use some special gases for some particular reason as well as filler rod can be used to join thicker metals.

There are three different polarities available in GTAW:

Direct-Current Electrode Negative (DCEN): Referred as straight polarity. Electrode is connected to negative terminal and metal is connected to positive terminal. In DCEN, 2/3 of power is located at the work end and 1/3 of power is located at the electrode. Relative narrow and deep welds are produced.

Direct-Current Electrode Positive (DCEP): Referred as reverse polarity. Electrode is connected to positive terminal and metal is connected to negative terminal. The heating effect is more at electrode, shallower weld is produced. The weld will be clean. This is employed mostly where we don't require much penetration.

Alternating Current (AC): The polarity will be changing with respect to time. Reasonably good penetration and clean weld obtained.

Low deposition rates, excessive currents can cause tungsten electrode to melt are the limitations of the process. Whereas getting clean weld, control on dilution rates are advantages.

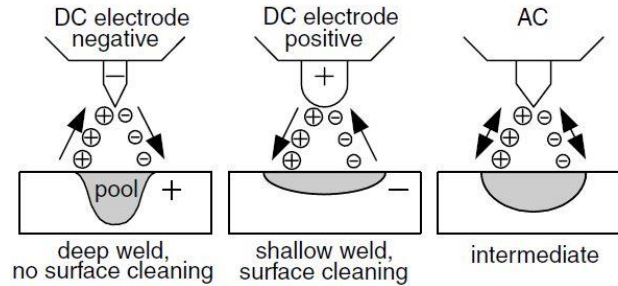


Figure. 2.1 Polarities in GTAW

Figure. 2.1 Three different polarities in GTAW [kou]

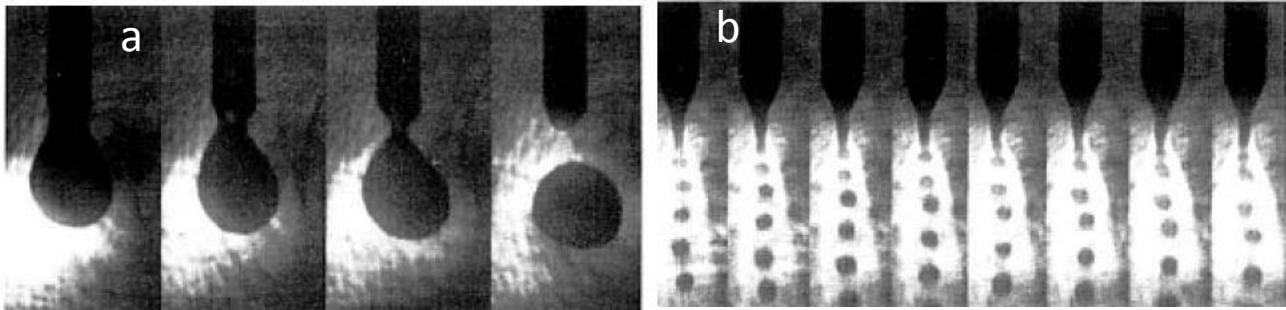


Figure. 2.2 a) Globular Transfer b) Spray Transfer [2]

Gas-metal arc welding (GMAW): Is the process which makes use the arc established between continuously fed filler wire and metal piece to heat, melt and join the metal pieces. Shielding of weld pool can be taken care by the inert gases: Helium, Argon etc. Mostly DCEP will be used in GMAW, as it is having the advantages of low spatter loss, smooth metal transfer, stable arc and good weld penetration.

There are three metal mode transfers, which are widely used:

Globular metal transfer: Which uses the principle of gravity. Often globular transfer is not smooth and produces spatter.

Spray transfer: Which uses the electromagnetic force. This is very faster, low spatter and smoother.

Short-circuiting transfer: Which uses the advantage of surface tension phenomenon. It uses lowest range of weld currents. Produces fast and freezing weld pools.

2.1.3 High-energy beam welding

This is the precision welding process, which uses high energy transferred in the form of either electrons or photons to melt the materials to join them. Today, high-energy beams, such as laser and electron beams, have been increasingly used in the industry for welding, cladding, and additive manufacturing. Due to the high-energy density and small beam size, gives us the characteristics of deep penetration, low heat input, small heat-affected zone, low thermal distortion and good dimensional accuracy and integrity. This processes are not cost effective as they require very high significant capital investment. Vacuum is required in electron beam welding, so as to prevent the dispersal of the focused electrons by collision with air or other gaseous or physical molecules. Which increases the capital investment. These processes are high power density but low energy-input process, provides solutions to a number of problems commonly encountered with conventional joining techniques. The principal characteristics of laser welding are: accurate positioning of the weld bead, rapid heating and cooling, low distortion and process flexibility. Sun and Ion showed that there is potential for its application in many industrial sectors [17]

. It is very difficult to join Ti/Al by conventional welding processes because their melting temperature difference is very huge, but laser welding provides an advantage to weld them.

2.1.4 Non-fusion welding processes

The processes in which melting is not responsible to make joint between two materials, called non fusion welding processes. Still heat can be used in these process, but for other reasons: to reduce power required to cause plastic deformation or to improve diffusion, may be both. There are many processes, who come under this class: Resistance welding, Friction stir welding, explosive

welding, brazing, soldering etc. As we are not dealing with these, it is out of our interest. However these processes having an advantage over fusion welding processes in joining dissimilar metals.

2.2 Processing Parameters:

η is the heat source efficiency.

$$\eta = \frac{Q}{Q_{nominal}}$$

Q is the rate of heat transfer from the heat source to the work piece, $Q_{nominal}$ the nominal power of the heat source. A part of power that we provided will be transferred to the work piece, other will be lost to surroundings, so $\eta < 1$ always. If we know η value then we can estimate the rate of heat transfer to the work piece.

In arc welding processes with constant voltage E and current I the η can be expressed as

$$\eta = \frac{Q}{EI}$$

The above equation can applied to high energy beam welding also, $Q_{nominal}$ in laser welding refers to the power of laser. In welding community, heat input refers to $Q_{nominal}$ or VI in arc welding processes. Heat input per unit length refers to the ratio of $Q_{nominal}/V$ or EI/V , where V is the weld speed.

2.2.1 Current

If the welding current is more than weld penetration is high as well, if the weld current is decrease then penetration is also comes down. Choubey et al. [18] increase in the heat input affects the micro-constituents of parent metal, heat affected zone and significant variation in the microstructure of HAZ of different positions.

2.2.2 Travel Speed of welding torch

As travel speed increases, the amount of time that the arc is over a particular point along the joint is less and the resulting level of penetration decreases. As travel speed decreases, the amount of time that the arc is over a particular point along the joint is greater and the resulting level of penetration increases

2.3 Effect of welding parameters on weld pool shape

“The size and, especially, the shape of the melt region in a fusion weld affects the mechanics and kinetics of solidification and the structure and properties of the resulting weld” (2). The shape of the melt pool is a function of material thermal properties, welding speed, and welding power (voltage times current).

If the thermal conductivity of the material is high, then we observe small welds. As the given heat input will be spread over the material, takes longer time to reach melting temperature.

For a given heat input, the lower the melting temperature, the larger is the melt pool size.

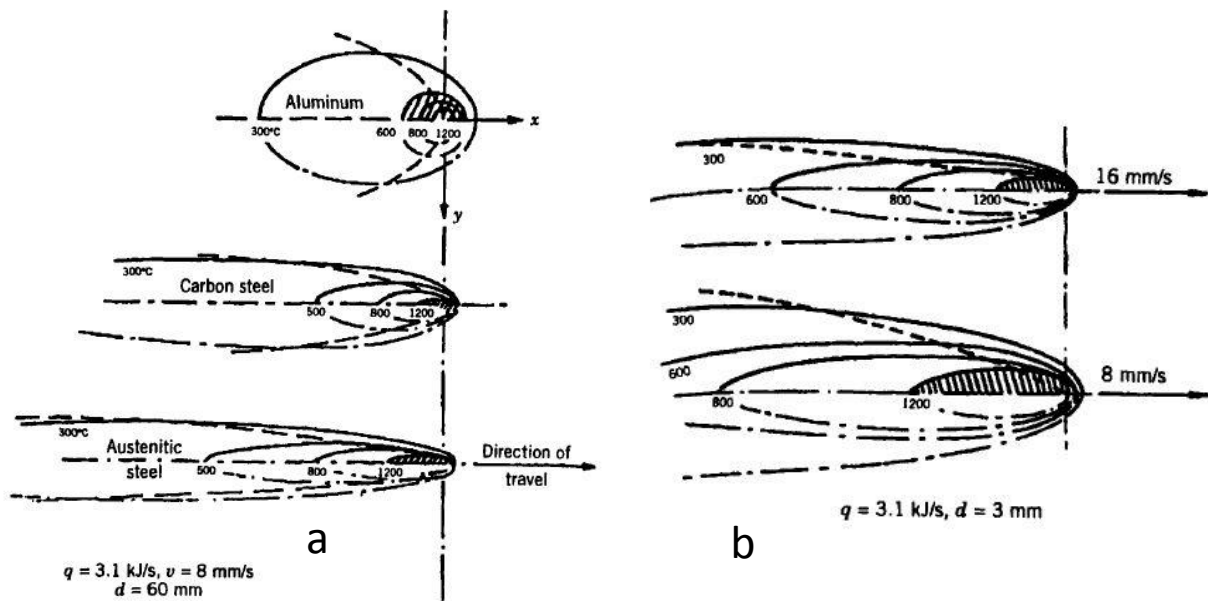


Figure. 2.3 a) effect of thermal conductivity of a base metal on weld pool and surrounded HAZ
 b) effect of speed of welding on weld pool and surrounded weld pool. [1]

Welding velocity effects both the size of the weld pool as well as the surrounding heat-affected zone (HAZ). When the weld is stationary, the top view of the weld is round, approximately hemispherical in three dimensions. Once the heat source starts moving melt pool turns into elliptical plan form and prolate 3-D hemispherical shape. At certain critical velocity they attains a specific tear drop shape with a tail at the trailing end of the weld pool, from the elliptical shape. The critical velocity depends on the material. Still, if, we are increasing the velocity tear drop shape elongates more and more, reduces the width of melt pool and HAZ. At very high speeds, the tail of the tear drop shaped melt pool can detach, isolate regions of weld pool and lead to shrinkage-induced crack at center line of weld pool. We could see the change in weld pool shape with thermal conductivity as well speed of torch in Fig. 2.3

The increase in thickness makes the weld pool smaller.

For a given heat input, weld material, geometry: Increase in the energy density increase the efficiency of melting, thereby increasing the melting, especially in depth direction.

2.4 Heat flow in the welds

The welding industry mostly concern about the problems of distortion, residual stresses, and reduced strength of a structure in and around a welded joint. These problems are the result of the thermal cycle caused by the localized intense heat input of fusion welding. This is very important to know or understand about the solidification rate, maximum temperature reached, temperature profiles in weldment which affects the residual stresses, distortion, size of HAZ. In the past there were many attempts made to model theoretically the thermal cycles, tried to get simple equations from the available experimental heat transfer data. Out of many, Rosenthal's simplified generalized equation of heat flow is widely accepted till date, but has some draw backs. Nevertheless drawbacks of the model, it will create a basic idea about the heat flow in the weld.

2.4.1 Rosenthal's heat flow model.

The analytical model of Rosenthal in the late 1930, by making use of basic Fourier heat flow equation and implying it to moving heat source is most popular for calculating the thermal history of welds. Assumptions (i) Quasi or pseudo-steady state of heat transfer, (ii) Energy input from the heat source was uniform and moving with a constant velocity. (iii) Heat source is a point source, all the energy giving is deposited into the weld at a single point. (iv) Thermal properties of the materials are constant and moving coordinate system is assumed.

Main drawback of the model is, it completely neglect the convection. It is purely conduction based heat flow model. Which will not give accurate results.

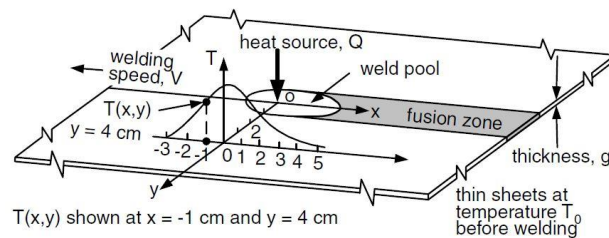


Figure 2.15 Two-dimensional heat flow during welding of thin workpiece.

Figure. 2.4 Two-dimensional heat flow during welding of think work piece.[2]

Rosenthal's 2D heat flow equation:

$$\frac{2\pi(T-T_0)kg}{Q} = \exp\left(\frac{vx}{2\alpha}\right) K_0\left(\frac{vr}{2\alpha}\right)$$

T: melting temperature, T_0 : room temperature, k: thermal conductivity

g: thickness, Q: heat input per unit length, V: welding speed

α : thermal diffusivity, r: radial distance from origin $= (x^2 + y^2)^{1/2}$, K_0 : Bessel's modified equation

2.4.2 Goldak heat source

Double ellipsoidal geometry of heat source is assumed, which is versatile and flexible to handle non-axisymmetric cases such as strip electrodes or dissimilar metal joining. This has an advantage to model both shallow penetration arc welding processes and deeper penetration laser and electron beam processes. A detailed model was discussed in [19]. Which makes us to understand the advantages of this heat source over all the proposed models. Ellipsoidal sources are combined, the front half of the source is the quadrant of one ellipsoidal source, and the rear half is the quadrant of another ellipsoid. For validating the model Goldak et al. verified cooling time values of this FEM double ellipsoid model for both shallow and deep penetration. These are much closer to the experimental values than the Rosenthal's model.

2.5 Motivation for the present work

Engineering of weld microstructure: Chen Guoqing et al. [20] presented electron beam superposition technique to weld Bronze and Titanium. They first tried to join them by placing electron beam at center but at both the interfaces they observed IMCs. They understand the reason for it is Cu has not melted much. They shifted beam offset towards Cu and welded, now they observed IMCs at Ti interface. They combined these two steps together to join them and succeeded to join them without IMCs. This has driven me to study the solidification microstructure of the weld, which helps us to engineer the microstructure.

Literature on Ti/Ni systems [6, 7, and 9]: (i) First attempt was made by Steresky and Ryba. They showed that the joints are very brittle. Observed convection swirls in the weld pool, which was the result of poor mixing. (ii) Chatterjee et al. presented a detailed solidification microstructural analysis. In which they tried to explain the thermodynamic and kinetic conditions helped the IMCs to form in weld pool. They observed layers of IMCs at both the base metal interfaces. Recently Chen et al. could get the Ti/Ni laser welded crack free joints by optimizing the processing parameters.

Extensive work has been done on joining dissimilar metals since early 1930, which were mainly focused on joining them successfully without cracks, good mechanical strength and no intermetallic compounds in the microstructure, by varying welding parameters (heat input, velocity, offset distance etc.). Available literature didn't discuss or showcase the details about average weld pool composition, melt ratios by varying welding parameters and effect of them on microstructure, which has direct relationship with the mechanical properties of the joint. Asymmetric weld pool observed because of differential melting of base metals, even heat source applied symmetric on two plates [21].

We can't get average composition of weld pool of Ti-Al joint, less than 20 %At Al, by any combination of processing parameters [22], which gives us a clue that average composition is a function of processing parameters. Chen et al. [8] have given the details of melt ratio variation with welding parameters by analytically modelling Rosenthal two dimensional equation but didn't discuss and relate them with microstructural changes. As these two papers strongly supporting the argument that processing parameters effects average weld pool composition.

Microstructural variation was not there much and the composition of weld metal was independent of heat input [23]. The influences of heat input on the microstructure of the fusion welding join are not significant [24], but $TiAl_3$ observed at joint interface in case of low heat input, $TiAl_3$, $TiAl$, Ti_3Al were observed at joint interface during high heat input. Fracture was observed in fusion zone in low heat input and at interface in high heat input. Which directly imply that intermetallic formation is sensitive to heat input and indirectly motivates that heat input has an effect on average weld composition. The result of the XRD patterns in low heat input joints, intermetallic $TiAl_3$ phase is formed at the interface besides α -Ti, β -Ti, Al, and Si and in high-heat input joints, which

are identified as $TiAl_3$, Ti_5Si_3 , $TiAl$, and Ti_3Al . Which is evident of more melting of Al alloy with increasing heat input.

The plate thickness and the laser power have important influences on the distribution of the Cu element in the intermixing zone [25]. Even though they didn't compare with many number of combinations but Cu dissolution has shown huge variation with varying plate thickness and heat input. Plate thickness 7mm, laser power 8KW combination melted ~35.6 %at Cu, whereas 10mm thickness, 11KW laser power combination melted <1 %at Cu.

Many experimental studies were done to optimize the offset distance, heat input to get a good weld joint between dissimilar metals. We thought if we estimate the melt ratios by varying processing parameters by computationally, it would be so useful to design any welding experiment.

Schubert et al. [26] has observed with increasing laser power key hole mode melting was observed in Ti6Al4V, Lead joint. As lead started evaporating helped the keyhole mode of melting. Which gives us a clue that with increasing heat input lead started melting more. They pointed out that controlling the diffusion mechanism appropriately by applying a lower heat input can reduce the formation of brittle intermetallic phases in dissimilar materials welds. Mai and Spowage [16], showed that controlling melt ratios can produce crack free joints.

Chatterjee et al. [6] observed the average weld composition as Ti-40%at Ni in Ti/Ni LW joints. They claimed that, as Ti has lower thermal diffusivity Ti melted less. The average weld composition of Ti/Ni EB welded joints [27], the average composition found as Ti-60%Ni. They have not provided any reasons for Ni rich weld pool. We believe that, EB welding applies more heat input than LW that might result in Ni rich weld pool.

These have motivated us to start our research on very basic thing, which is composition variation with respect to all the processing parameters, at the end which decides the microstructure or weld as well mechanical performance of joint.

2.6 Conclusions from Literature Review

We can clearly observe that the available literature is indirectly saying, there is a relationship between the average weld composition is a function of processing parameters. A detailed microstructural analysis for Ti/Ni joints is present in the literature, no extensive work was done to observe the microstructural changes by varying processing parameters.

2.7 Objective

Microstructural comparison Ti/Ni laser welded joint with a different welding speed than the reported laser welded joint by Chatterjee et al. [7]. Bringing out the correlation between the average weld composition to the processing parameters.

Chapter 3

Experimental Procedure

3.1 Laser welded sample processing conditions

The parameters used to weld Ti and Ni metals as well the observations are presented over table 3.1. The macroscopic observation is, the weld melted in keyhole mode.

Table 3.1 processing conditions used during laser welding of Ti/Ni

Power (kW)	Speed (mm/min)	Focusing condition	Comments
5	0.5	In focus	Key hole, good

3.2 Equipment used

Electro discharge machine (EDM) was used to cut a small sample from total weldment for characterization. Manual polishing machine were used to polish the sample to remove the surface roughness. Powder X-ray diffraction was used to know the phases that are present in the weld pool. Microstructural characterization was done using Optical microscope and Field emission scanning electron microscope (FESEM).

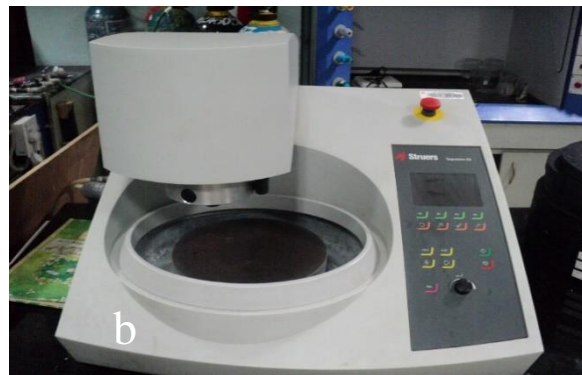


Figure. 3.1 a) Manual paper polishing machine. b) Manual cloth polishing machine



Figure. 3.2 a) Optical Microscopy



b) Scanning electron microscopy

3.3 Experimental steps involved

Processing parameters for the laser welding of Ti/Ni are mentioned in table 4.1. We have cut the sample of thickness 3mm in transverse direction from the weldment, which is representative of total weldment. To characterize it through X-Ray diffraction (XRD) we have cut the sample in such a way that, only weld pool will be characterized. To do that, we have machined most of the base material around the weld pool. Polished the sample with 500 to 2000 grit papers, followed by polishing it with 9 μ m, 6 μ m, 3 μ m, 1 μ m diamond suspension and washed the samples with Methanol. $\theta - 2\theta$ scan in the range of 0-120 $^{\circ}$ was done. Microstructural characterization was done by Optical microscope and FESEM. To observe microstructure under Optical and FESEM, after finishing 1 μ m polishing, sample was etched with 10ml HF, 25ml HNO₃, and 150 ml H₂O for 2 minutes. Then observed the microstructures under Optical microscope as well in Scanning electron microscope. In FESEM by varying the working distance from 5-15 mm at EHT-15KV microstructural characterization was done. Composition was measured using EDS analysis was done to identify the phases in microstructure, at 6mm working distance and EHT - 15KV.

3.4 Computational details

Mat lab is used to solve Rosenthal's 2D equation (discussed in section 2.4) for temperature profiles for dissimilar metal joints. By assuming the geometry as one side is Ti thermal properties and other side as Ni thermal properties. Heat flux at the interface is averaged to get the total flux. By calculating the width of contours of melting temperature, measured the average weld composition of the melt pool varying heat input.

To calculate the area of each metal melted we referred the formulas mentioned in [8]. From area, we converted them into area fraction. The conversion from area fraction to composition is given below.

$$\text{Composition of A (\%at)} = \frac{Af_A * \rho_A * A_B}{Af_A * \rho_A * A_B + Af_B * \rho_B * A_A}$$

Where Af: area fraction, ρ : density, A: atomic weight

3.5 Algorithm for solving heat conduction equation through ANSYS APDL

Figure is the flow chart that shows the steps we followed to implement to solve fourier heat conduction equation by FE method by ANSYS.

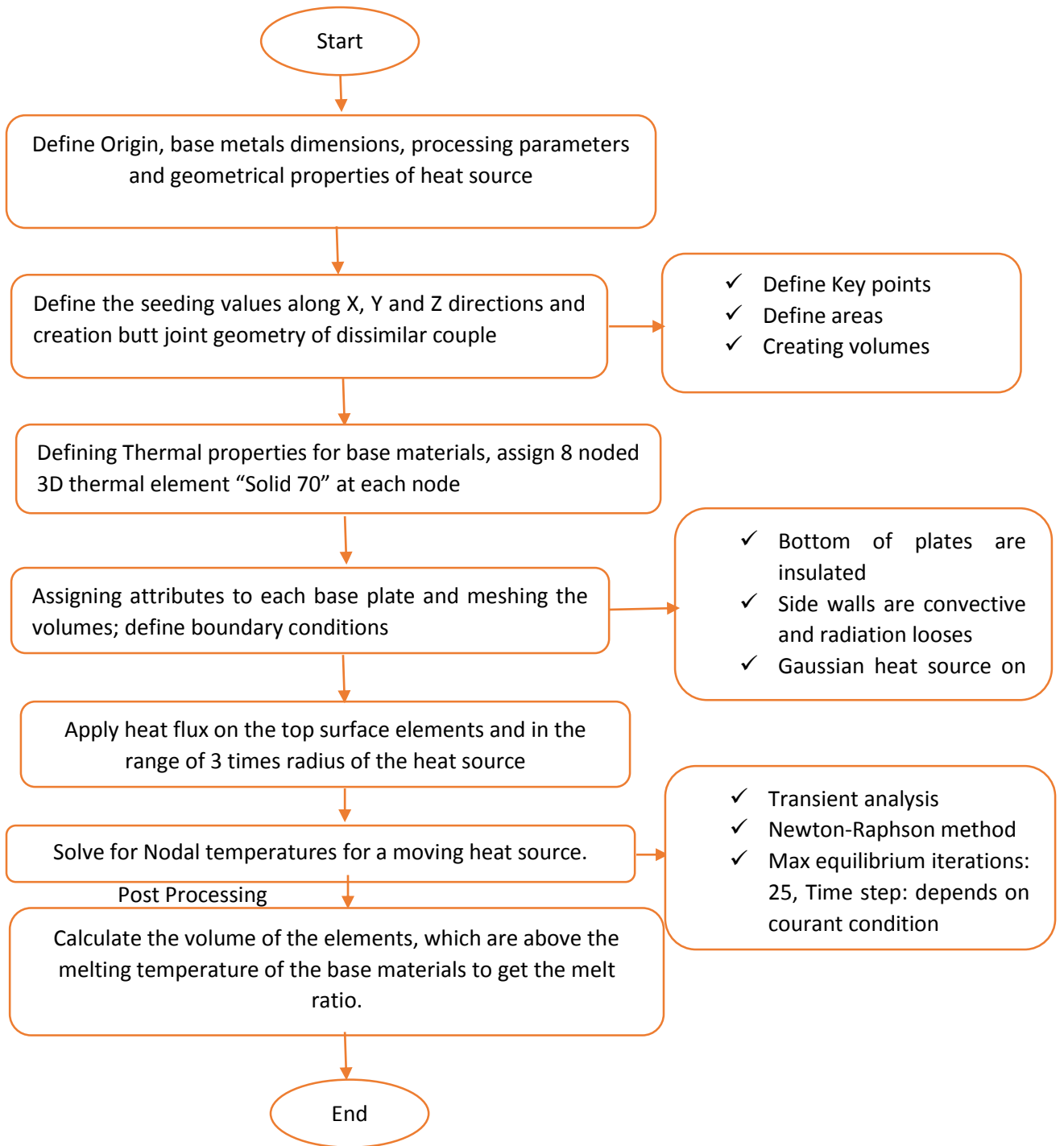


Figure. 3.3 Flow chart of algorithm used to implement FEM in ANSYS

3.6 Computational data

Tables 3.2, 3.3 and 3.4 shows the material properties as well processing conditions used in simulation for getting nodal solution in ANSYS.

Table 3.2 Material thermal property data for Copper [34]

Melting Temperature (K)	1358
Thermal Conductivity (W/m K)	$-0.0002T^2+0.0096T+393.688$
Specific Heat (J/Kg K)	$4.6515071*10^{-9}T^3-4.9657144*10^{-5}T^2+0.143199T+376.7528$
Emissivity	0.015

Table 3.3 Material property data for Nickel [34]

Melting Temperature (K)	1758
Thermal Conductivity (W/m K)	$7.196*10^{-12}T^4+4.99710^{-8}T^3+1.185610^{-4}T^2-0.1097862T+90.420288$
Specific Heat (J/Kg K)	$7.1961*10^{-12}T^4-4.997*10^{-8}T^3-1.63786*10^{-4}T^2+0.2895T+452.725$
Emissivity	0.03

Heat transfer coefficient ($W/m^2 K$), calculated at every temperature by formula:

$$24.1*10^{-4}*emissivity*T^{1.61}$$

Table 3.4 Processing parameters used in modelling

Laser power (KW)	2
Efficiency	0.23
Laser speed (mm/s)	10
Laser diameter (mm)	0.5
Mesh size	50*50*50
Time step (Sec)	6.67e-5

From Fig. 3.4, we can observe the geometry of butt joint and Gaussian heat source applied as well boundary conditions.

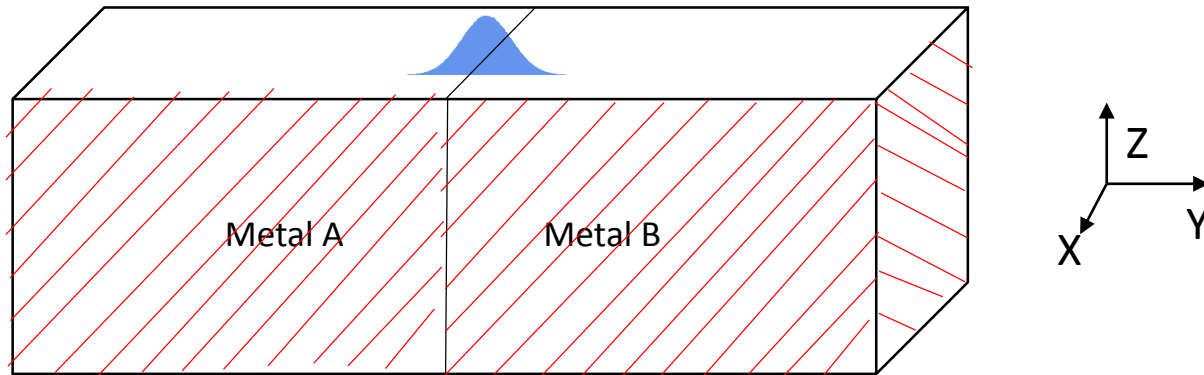


Figure. 3.4 Butt joint configuration, boundary conditions applied

Stability condition for explicit finite difference method:

$$\frac{\alpha \Delta t}{(\Delta x)^2} \leq \frac{1}{2n}$$

α : Thermal diffusivity, Δt : Time step, Δx : Mesh interval, n : 1, 2 or 3 for 1D, 2D or 3D, respectively

Chapter 4

Results and Discussions

In this section we presented the results of calculated average composition of the weld pool and compositional variation in the weld pool. The average weld pool composition was measured by considering melted areas in Ti and Ni base plates as triangles and converting the melting ratio thus obtained into composition. We showed the θ - 2θ scan of XRD, from which we identified the phases that are present in the weld pool. Microstructural variation in the weld pool is presented, which was done by FESEM.

4.1 Average weld composition

Figure 4.1 is the equilibrium phase diagram of Ti/Ni binary couple, which shows us the phases exist at particular composition and temperature. Figure 4.2 is the secondary electron micrograph of the weld cross-section at lower magnification, showing an asymmetry in the weld pool shape as expected in dissimilar couples. We can observe that titanium (Ti) has melted more than nickel (Ni), even though nickel melting temperature is lower than titanium. Ti has much lower thermal conductivity than Ni which promotes more localized heating and melting in Ti. We can see the composition variation throughout the weld pool from left to right. We calculated the area of Ti and Ni base metals melted and then calculated the average composition of the weld pool. The average weld pool composition found to be Ti-49.4%Ni. This gives us a clue that all the reactions are happening at this composition. From the phase diagram (Fig. 4.1), we can see that of this average composition corresponds to a mixture of TiNi and Ti₂Ni phases at equilibrium.

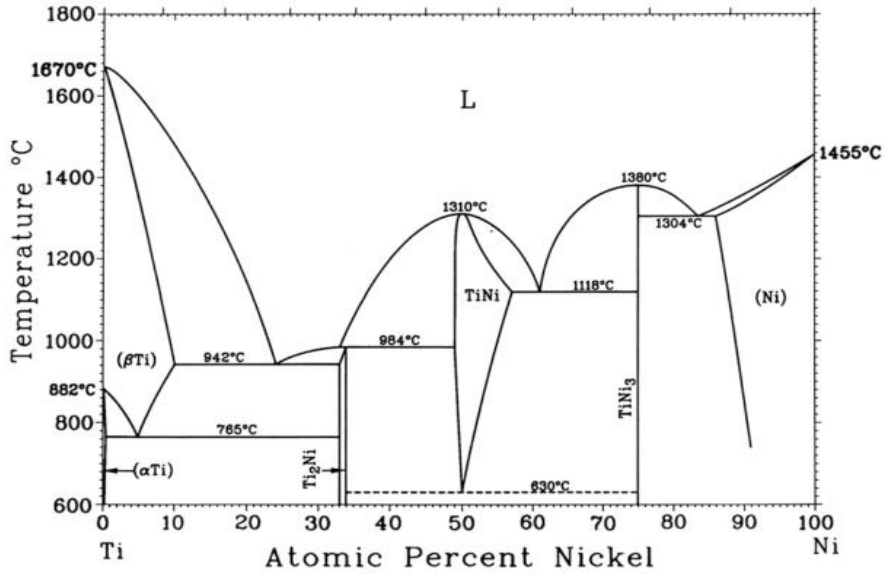


Figure 4.1 Phase diagram of Ti/Ni binary couple

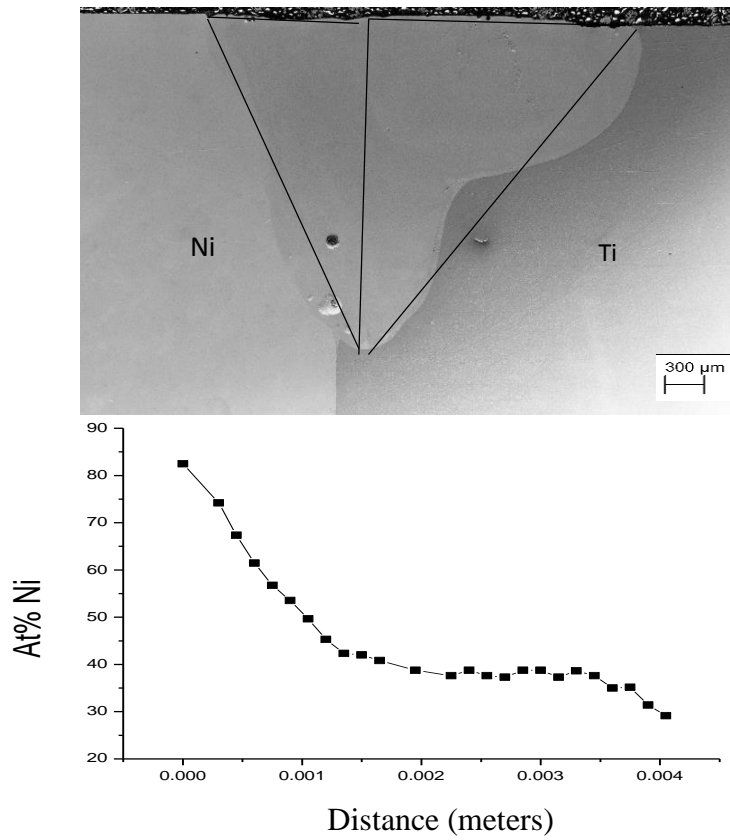


Figure. 4.2 Asymmetric weld pool with compositional variation

4.2 XRD Analysis

Powder diffractometer was used to know the phases that are present in the weld pool. We cut the sample in such a way that we can only scan weld pool area. A mirror finish polished sample (only weld pool) was scanned in 5° - 120° range. Data was collected and plotted intensity versus 2θ . The result of XRD analysis is showed in Fig. 4.3. The peaks in Fig. 4.3 were compared with ICDD patterns available. We considered all the phases that are present in the phase diagram as well compounds that are possible with the combination of Ti and Ni. We compared their three peaks of maximum intensity with result that we got. Many peaks are overlapping, as they have their maximum intensity peaks at almost same 2θ value. Although we cannot say that the peaks that we observe in the XRD should be there in the weld pool which needs other characterization technique to confirm it. From the XRD results we can observe the phases that are present in the weld pool are TiNi (monoclinic), TiNi (cubic), Ni₂Ti, Ti₂Ni, Ni and Ti. As we expected from the average composition result that our weld pool mostly consists of TiNi and Ti₂Ni. We do observe these phases, but in addition, we also see non-equilibrium phases TiNi (monoclinic) and Ni₂Ti, which suggests non-equilibrium solidification of the weld pool. We can see from Fig.4.4 that as atom% Ni is increasing the martensitic transformation temperature from monoclinic to cubic is rising. From the calculated average composition, the weld pool is richer in nickel content; this can be the reason to observe both cubic and monoclinic together. Moreover, with time TiNi transforms many non-equilibrium phases; which may be the cause for observation of Ni₂Ti [30]. According to the weld composition, we shall not see any monoclinic phase but still we are observing because of local compositional fluctuations. We can observe Fig. 4.2 that composition is varying from one point to another. In dissimilar metal welds the phase nucleating assumes significance according to the local equilibrium conditions present.

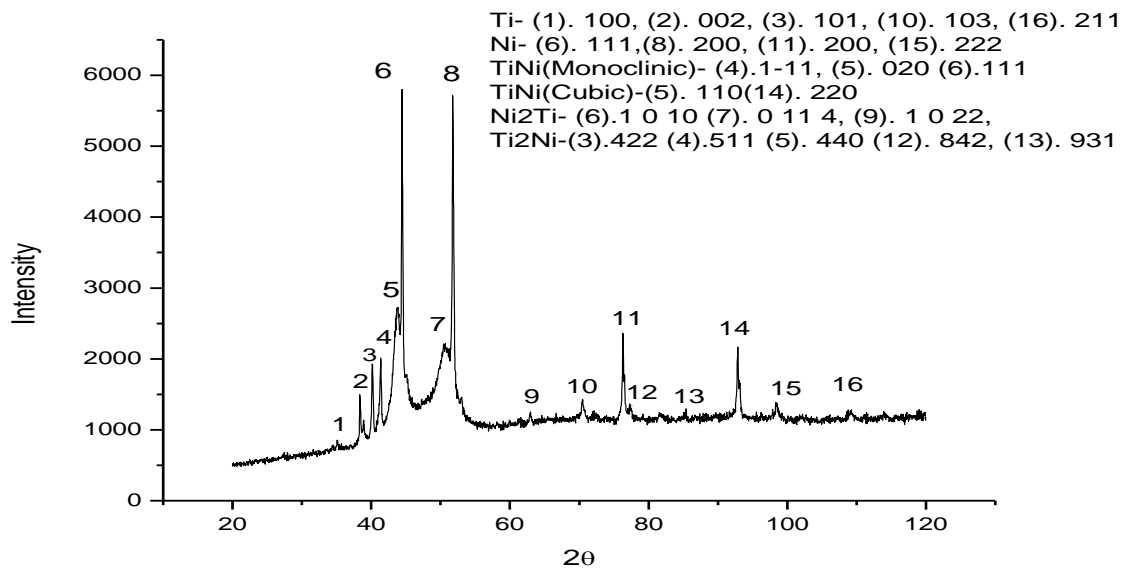


Figure 4.3 plot between Intensity VS 2θ

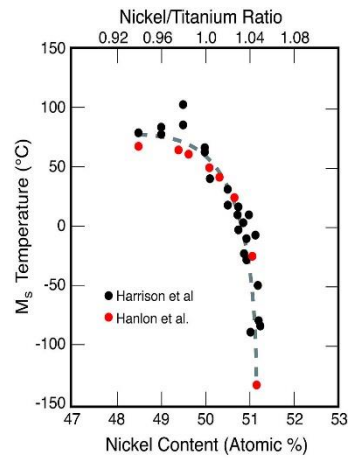


Figure 4.4 M_s temperature variation with respect to Nickel content [31]

4.3 Microstructural Analysis

In this section we showed the microstructural variation at different positions of the weld pool of weld cross-section. The sample was fine polished and etched to observe the microstructure in the SEM. All the images are secondary electron micrographs.

4.3.1 Ti Interface

In this section we showed the microstructure at Ti interface. We tried to portrait the microstructural features at Ti interface. We tried to understand the reasons behind these features. Secondary electron micrographs at Ti interface are shown in Fig. 4.5, EDS analysis identified, the phases present are: Ti_2Ni dendrites and Ti_2Ni+Ti eutectic mixture. Ti_2Ni are growing towards Ti base metal side, which is quite surprising and not regular. Interdendritic liquid between the Ti_2Ni dendrites solidified as eutectic mixture of $Ti+Ti_2Ni$. We could see that some base metal grains growing into the weld pool but could not because Ti_2Ni dendrites are coming towards Ti base metal side, which is heat extraction direction and suppressed them. This is quite surprising as dendrites should grow opposite to the heat extraction direction but here we are observing opposite to it. At the interface we can see a steep compositional gradient (from Fig 4.1); this makes Ti base metal grain growth difficult into the weld pool. We observed some grains tried to grow but the Composition at the Ti interface is rich in Ni content, which makes Ti base metal grains to feel completely different atmosphere. Moreover Ni solubility in Ti is very less (<1 at %). The conditions at Ti interface reflects the conditions of solutal melting [32] which melts the Ti base metal grains, which are already nucleated rather than helping them to grow into the weld pool. Meanwhile at a distance away from the weld pool Ti_2Ni phase has nucleated and started growing towards base metal, which stopped the base metal grains growth into weld pool.

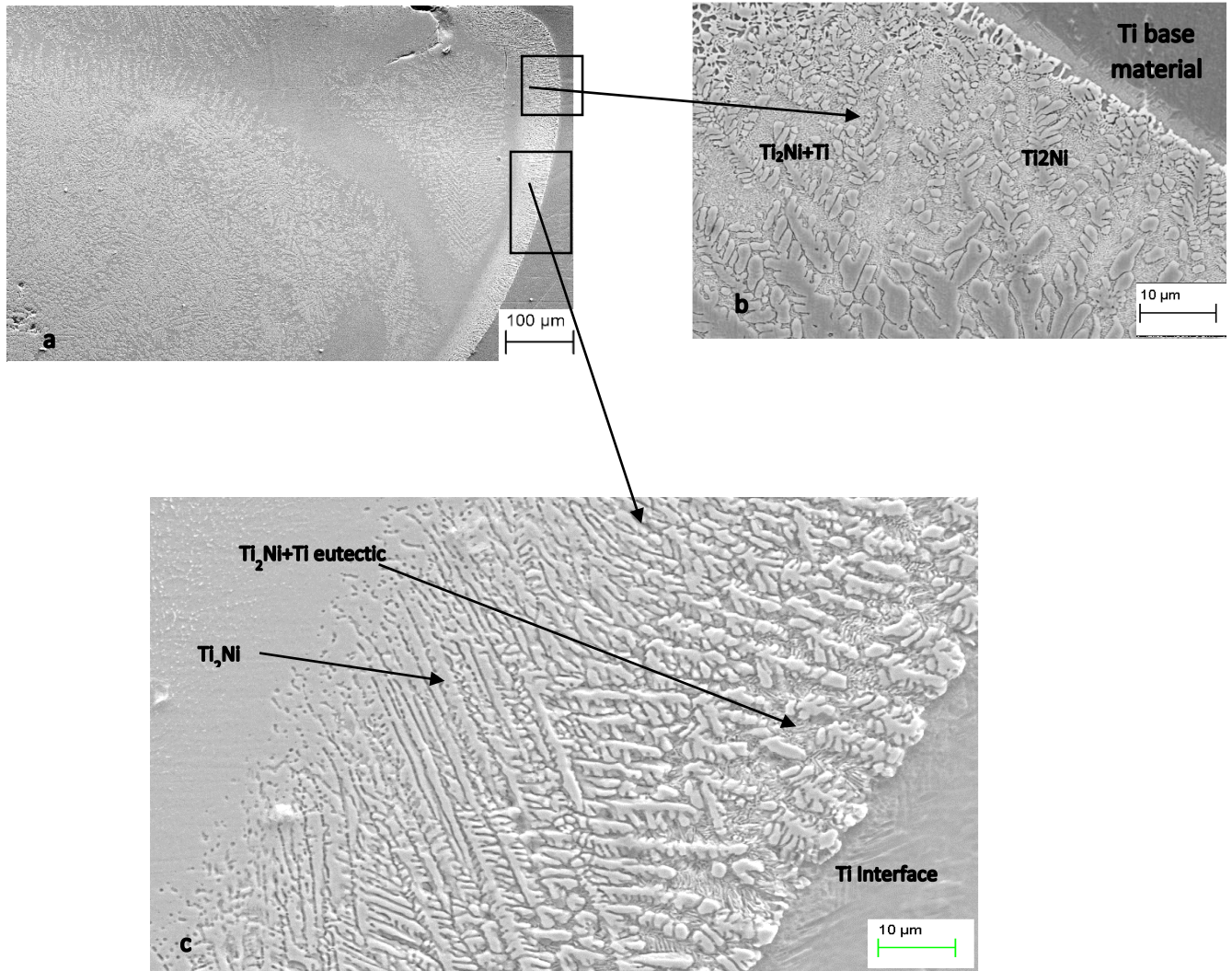


Figure 4.5 a) Ti interface at low magnification (b, c) at higher magnification of Fig. (a) which shows Ti₂Ni dendrites growing towards the Ti base metal interface

4.3.2 Ni Interface

In this section we showed the microstructure at Ni interface. We tried to portrait the microstructural features at Ni interface and we tried to probe the reasons behind these features. Secondary electron micrographs at Ni interface are shown in Fig. 4.6

At Ni interface, Fig. 4.6, we can observe three zones that are running parallel to Ni interface. From the EDS analysis, we identified that first zone consist of (Ni) and Ni_3Ti faceted dendrites have formed on (Ni) layer. Second zone is consist eutectic mixture of $\text{Ni}_3\text{Ti}+\text{TiNi}$ growing towards weld pool and faceted Ni_3Ti dendrites. Surprisingly we did not observe $\text{Ni}+\text{Ni}_3\text{Ti}$ eutectic mixture. Third zone consist of TiNi dendrites growing towards weld pool as well as Ni interface. Effect of Rapid solidification (RS) at Ni interface is very high as Ni has high thermal conductivity. This can be attributed to many consequences that are happening at Ni interface. We did not observe pre-existing Ni base metal grains growing into the weld pool, but fresh nucleation of (Ni) on partially melted pure Ni grains. Although maximum equilibrium solubility of Ti in (Ni) is 13.9 at %, we have found that it contains up to 18-23 at % Ti which can be attributed to increased solubility during RS. The figure also shows a region where the (Ni) + Ni_3Ti eutectic can form after the (Ni) phase field. However, we observed in Figure 4.6 (1) that a layer of Ni_3Ti that has grown over the existing (Ni) layer in preference to a coupled eutectic microstructure of (Ni) + Ni_3Ti . Kinetic problems in co-operative growth during RS can be the reason for the absence of $\text{Ni}_3\text{Ti}+\text{Ni}$. TiNi dendrites can form (because of composition and temperature gradient) at some distance away from the interface, by leaving the second region in the liquid state because the eutectic $\text{Ni}_3\text{Ti}+\text{TiNi}$ has lower variant temperature (to cool to that temperature it may take some time). Meanwhile TiNi could have nucleated and started growing all directions (Fig. 4.7) in the liquid. Later $\text{Ni}_3\text{Ti}+\text{TiNi}$ eutectic has formed.

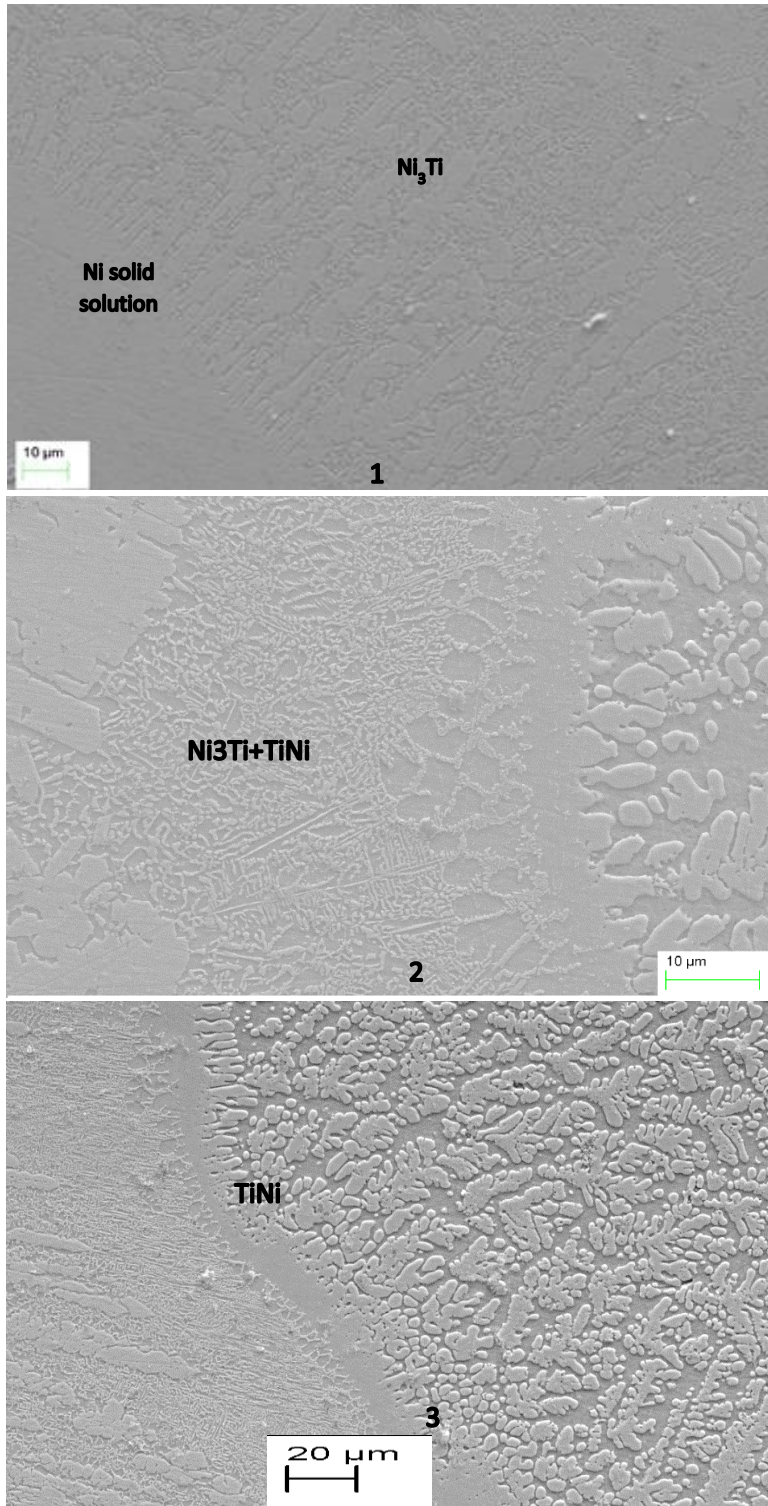


Figure. 4.6 (1, 2, and 3): Three zones at Ni interface



Figure. 4.7 TiNi dendrites growing in both directions

4.3.3 Middle of the Weld pool

We have shown the microstructural features in the middle of the weld pool.

When we observe the microstructure in the weld pool. EDS analysis identified it is full of Ti_2Ni and TiNi dendrites. We could see fine and coarse dendrites of TiNi bands in the middle of the weld pool in Fig. 4.8 a. occurs due to non-equilibrium effects of RS like solute trapping, growth velocity approaching the absolute stability limit and loss of interface equilibrium [6].

We have observed TiN phase on TiNi dendrites, in Fig. 4.8 b. Although we cannot confirm it by EDS analysis, but Chatterjee et al. [6] also have showed the same. They claimed that because of not using any protective gas during the process of welding, Nitrogen from the atmosphere diffused into the weld and formed TiN dendrites mostly on top of the weld pool.

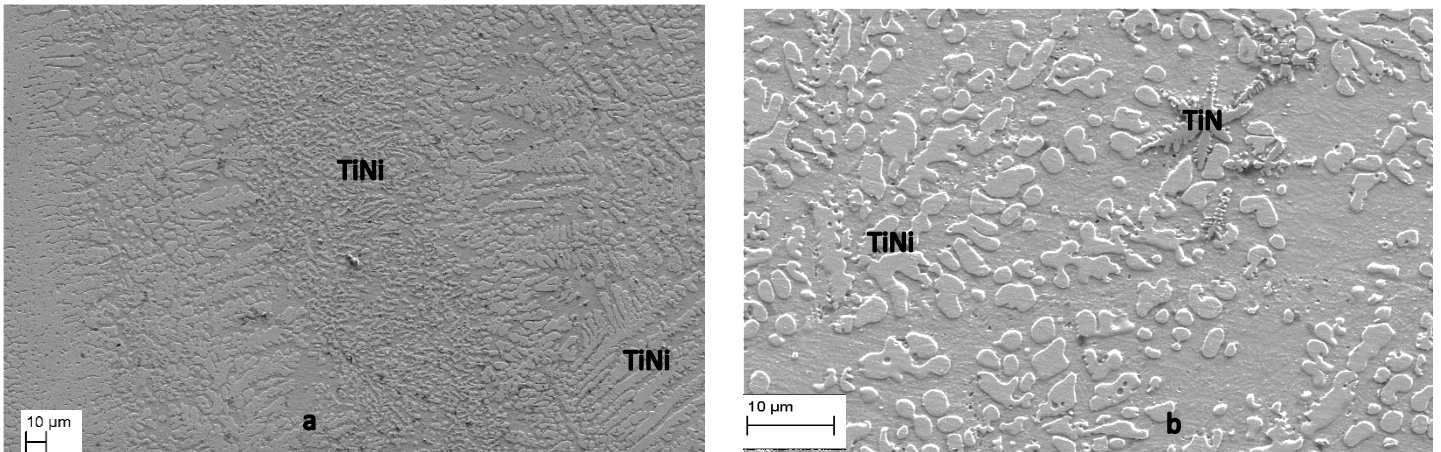


Figure 4.8 Middle of the weld pool. a) Fine and coarse bands of TiNi b) Impurities of TiN on TiNi dendrites

4.3.4 Bottom of the weld pool

Microstructural features of the bottom of the weld pool can be seen in Fig. 4.9. If we observe the microstructural features at the bottom of the weld pool (Fig. 4.10), we could see a block TiNi dendrites segregated because of density gradient in the liquid during solidification. Although macrosegregation is very common in solidification of castings where the fluid flow is mainly governed by buoyancy forces. In high energy beam welding it is rare to observe the density driven flow over surface energy driven flow [33]. However, for dissimilar welding, density difference can become large enough to give rise to strong buoyant flow. As we can see from Table 3.3, liquid Ni is almost twice as heavy as liquid Ti, and this difference can be significant to act as a driving force for fluid flow. Bottom of the weld pool consist of TiNi and Ti₂Ni dendrites.

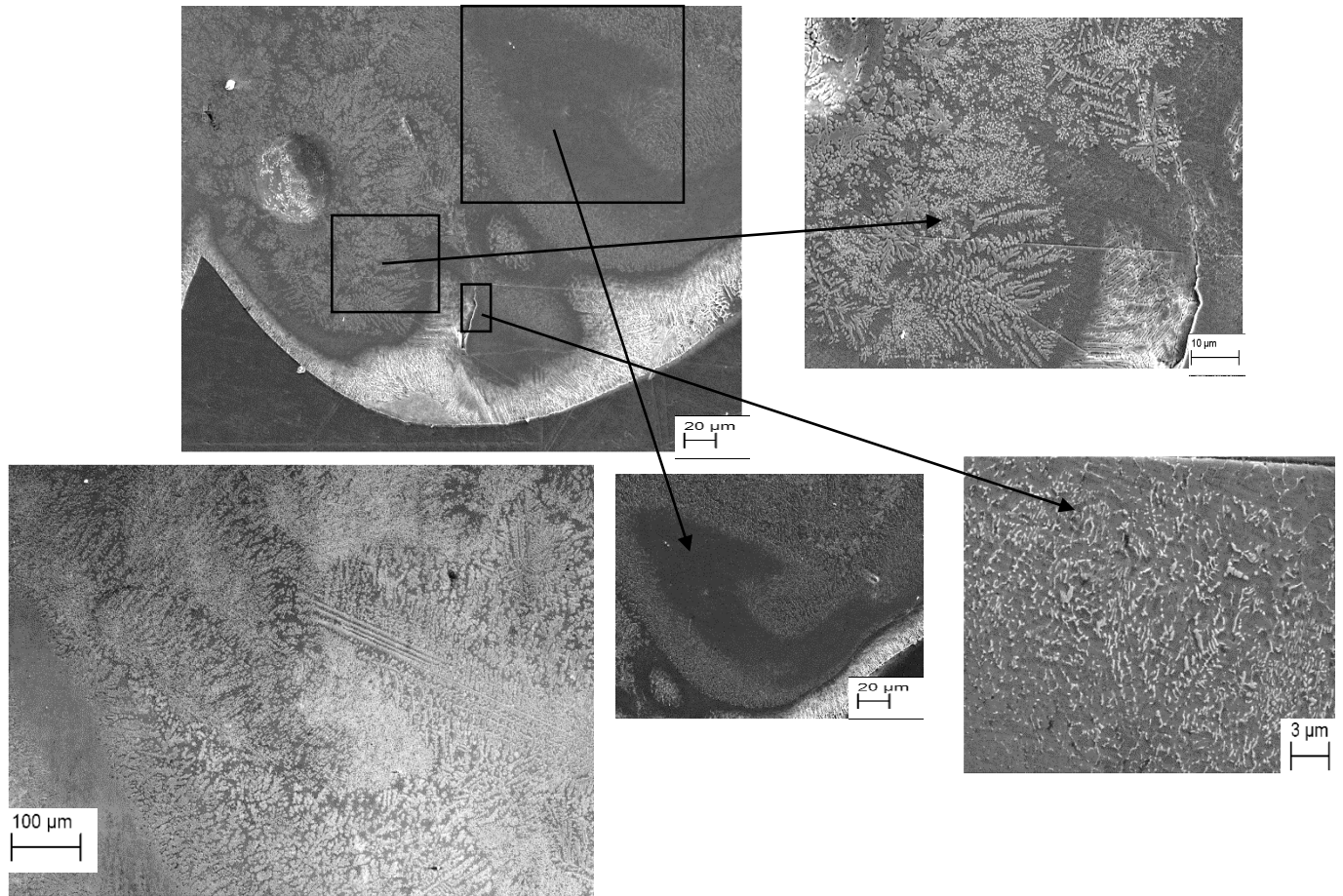


Figure 4.9 a) bottom of the weld pool, (b, c, d, e) magnified different portions of Fig (a).

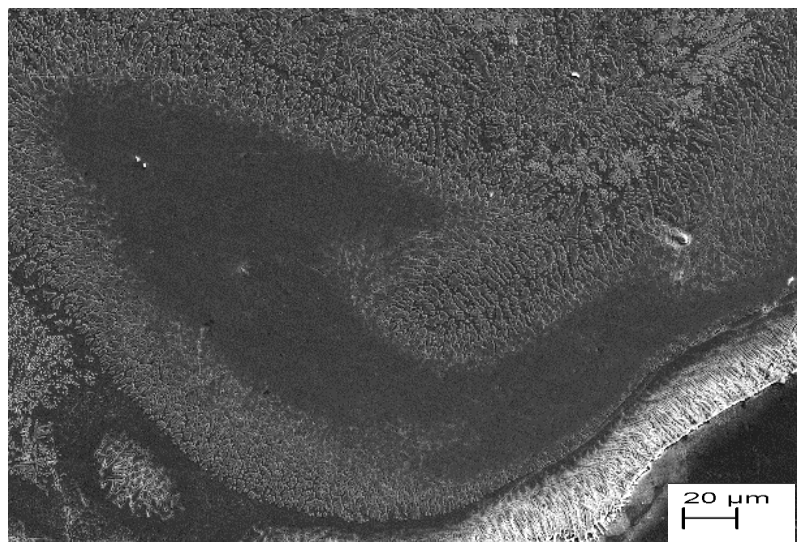


Figure 4.10 Block of TiNi dendrites segregated at the bottom of the weld pool

4.4 Computational Study

In this section we first present the results of Rosenthal's analytical model results. We have shown the variation of average composition of weld pool with respect to the heat input variation, then discussed about the accuracy of this model. Then tried to solve this by finite element model (FEM) which is more accurate and then shown the progress in results.

4.4.1 Rosenthal 2D equation

By solving Rosenthal's 2D equation, we drew temperature contours in Matlab. The thermal properties (thermal conductivity) for materials are taken at half of their melting temperatures ($T_m/2$). We followed the method followed by Chen et al. [8]. The details about Rosenthal's model is discussed in section 2.4.1. We averaged the heat flux at the interface. Solving Rosenthal's equation separately for each metal in dissimilar couple, then there we measure the width of melting temperature contour individually for Ti and Ni. Then we measured the volume melted then converted it into the average composition. We repeated this by varying heat input.

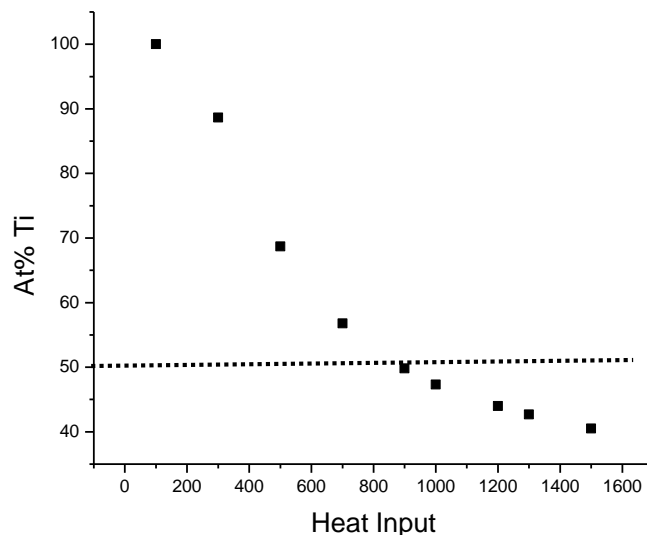


Figure 4.11 At% Ti variation with heat input (J/m)

Chatterjee et al. claimed that Ti is having lower thermal diffusivity compared to Ni, which resulted in Ti rich melt in laser welding of Ti/Ni dissimilar couple. But, as we are increasing heat input (Fig. 4.11) we could see a region which is separating the regions of melt rich in Ti and rich in Ni. As Rosenthal's model, is an assumption; we cannot say accurately that this result is so true. The drawback include: (i) Averaging of heat flux at the interface of dissimilar joints. (ii) Unable to incorporate temperature dependent thermal properties into the calculation. However, if we think back the reason for this result can be that, when we are increasing the heat input: melting temperature of the metal comes into picture. Even Ti has lower thermal diffusivity than Ni, the melting temperature of Ni is lower than Ti. There will be an interplay between all the thermal properties (discussed in section 2.3), at the end whosoever is dominant, the effect will be reflected in the average weld pool composition. This result is strongly agreeing with Chatterjee et al. [6], when they laser welded Ti/Ni joint they observed Ti-40 at% Ni. They claimed that, since Ti has lower thermal conductivity Ti melted more. But when they welded Ti/Ni joint by electron beam they observed Ni rich melt [29]. As electron beam impose high heat input into the base metals (electrons can interact with metals and absorptivity is high). This motivated us to move and cross check this result with more accurate model. This result motivated and gave a clue that average weld composition is a function both material properties as well as the processing parameters. If we are able to correlate them, then that would be great.

4.4.2 Finite Element Method

Thus we have chosen to solve heat conduction equation by finite element method. Steps followed to implement FEM in ANSYS have shown in Fig. 3.6

Nobody has attempted to observe the average weld composition with varying processing parameters in detail. This kind of study is absent in the literature, this gives a necessity to set benchmarks to our solution. This assures us that the solution we are getting is physical, we approached in three ways.

Symmetrical temperature contours

By imposing similar thermal properties in dissimilar butt joint geometry and applying heat flux at the interface, we should get mirror symmetrical temperature contours about the interface. As we can see Fig. 4.12 We have got symmetrical temperature contours about the interface.

Energy Balance

We need to solve for nodal solution, by giving all the input parameters (velocity, area of element, heat flux, density, specific heat, time step) as 1 and making thermal conductivity and film coefficient very less. The solution should give the temperature rise also 1K. We can observe the result of this simulation in Fig. 4.13 We got 1K rise in temperature which satisfies the condition $Q_{input} = Q_{output}$.

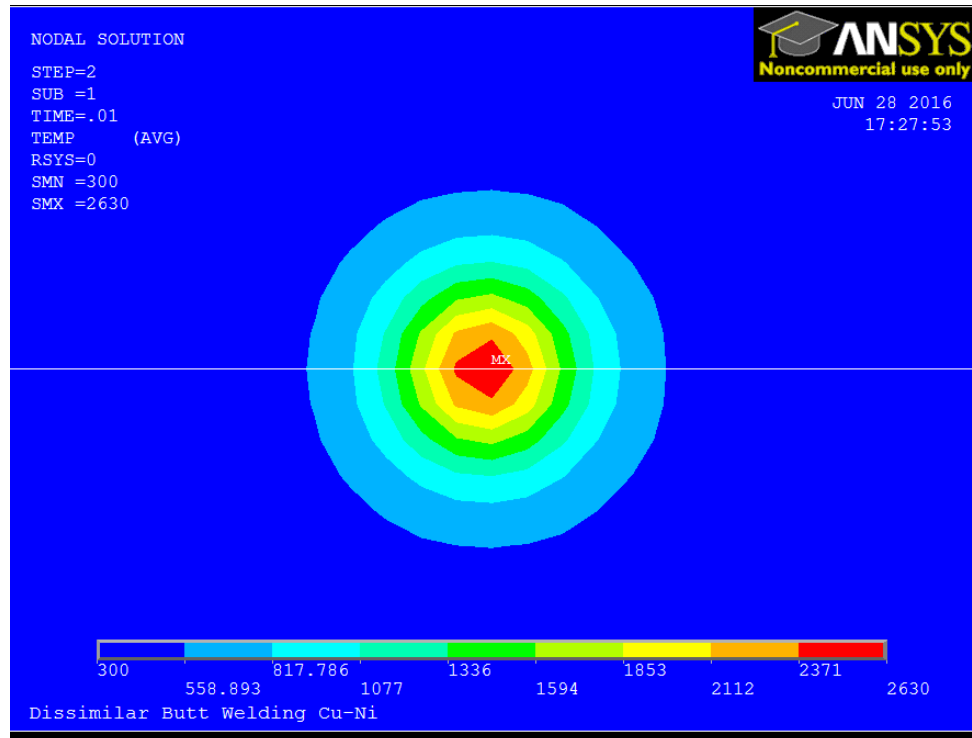


Figure.4.12 Symmetric temperature contours about the interface

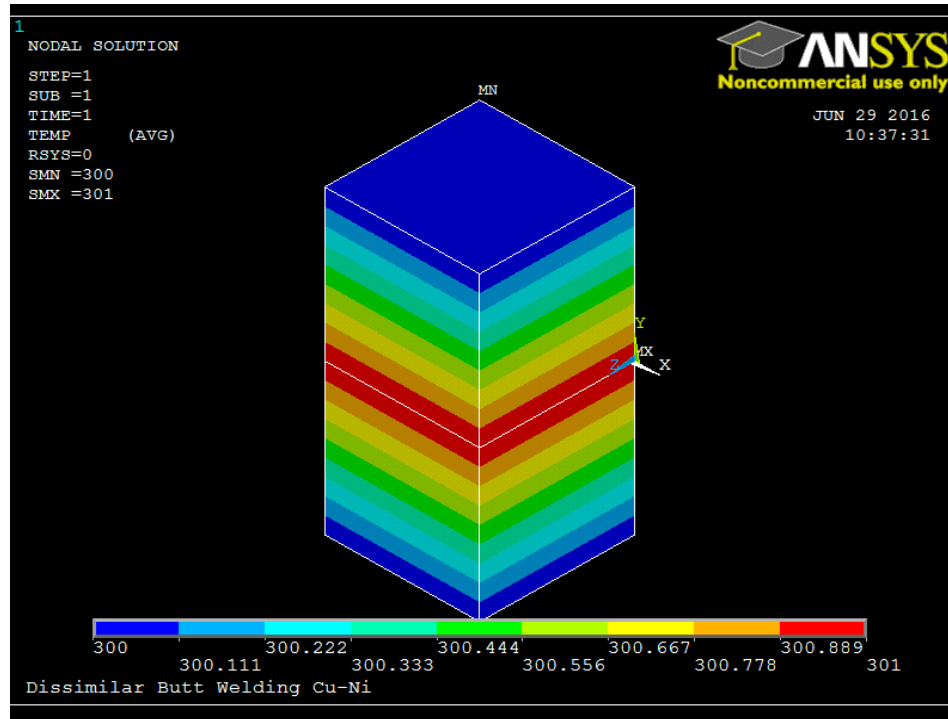


Figure. 4.13 1K rise in temperature by applying heat flux of 1J/m^2

Mesh Independent Study:

We have studied whether our solution is mesh independent or not, by varying mesh size. In this section we present the results of mesh independence. For this we have written the code in such a way that we will get the maximum temperature in each and every load step, then plot the maximum temperature in each of the load step versus the time. In Fig. 4.14 we can see the plot between the maximum temperatures versus time. We can observe the details of mesh size (50*50*50 says that each of dimensions have divided into 50 partitions, similarly others also. For this simulations we considered all the dimensions are same) used as well the courant number (CN) for that simulation used. We can observe the maximum temperature reached in each of the mesh size is almost same and the solution is oscillatory stable.

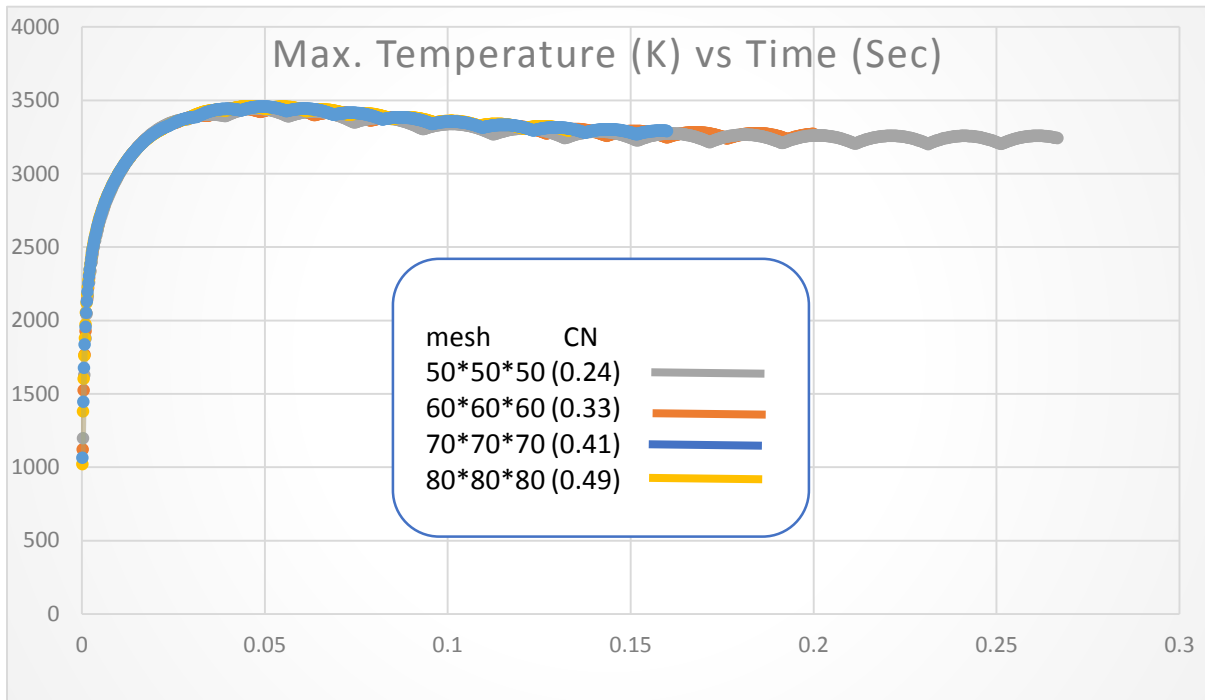


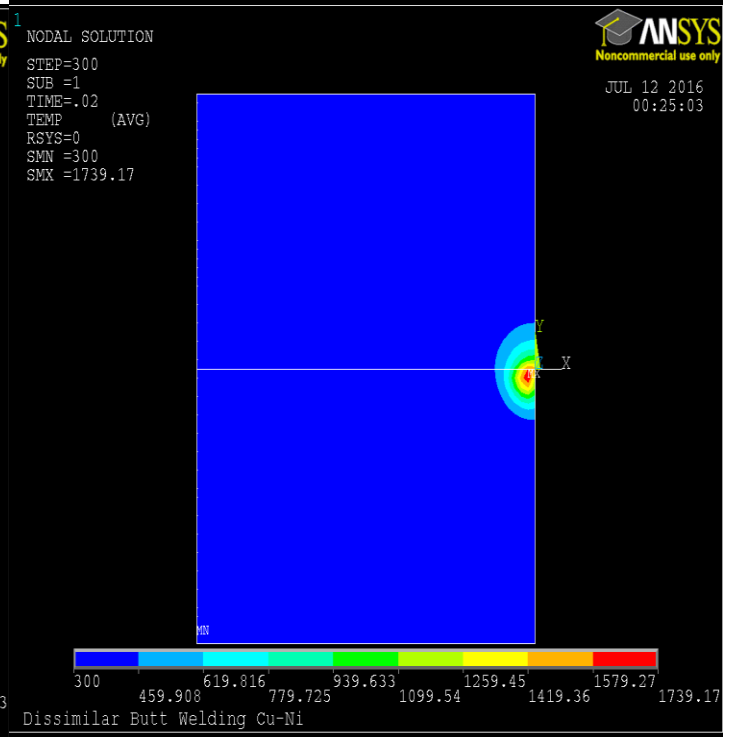
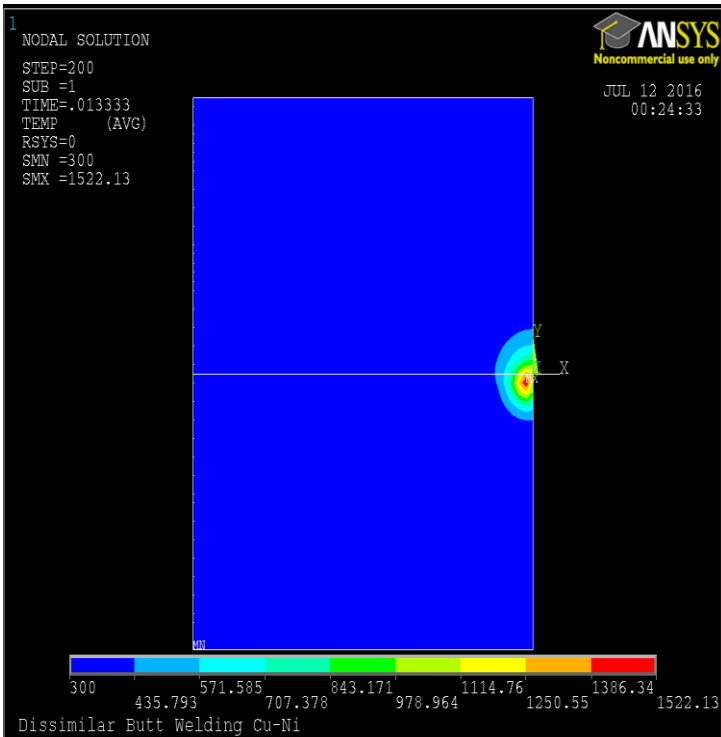
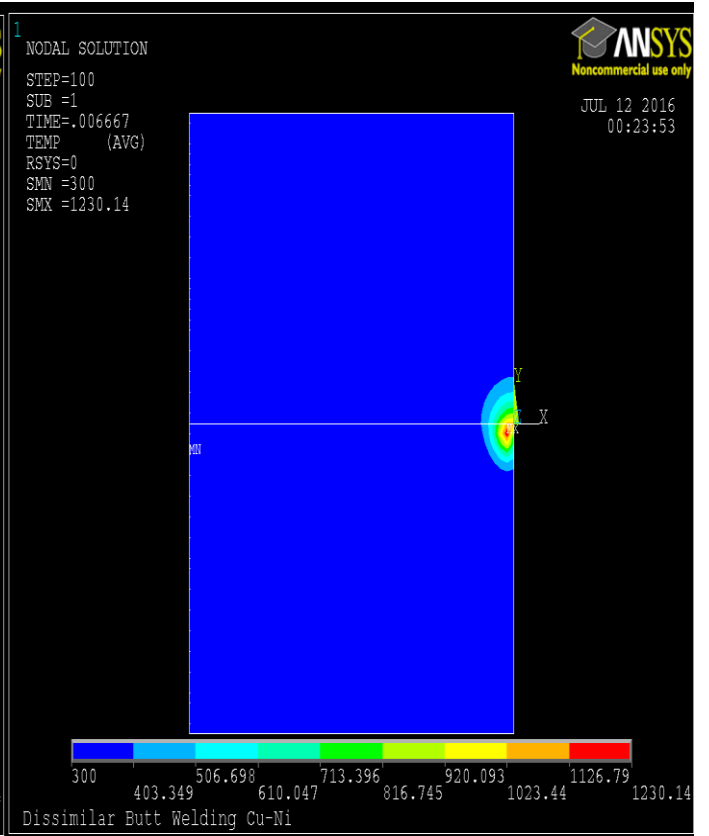
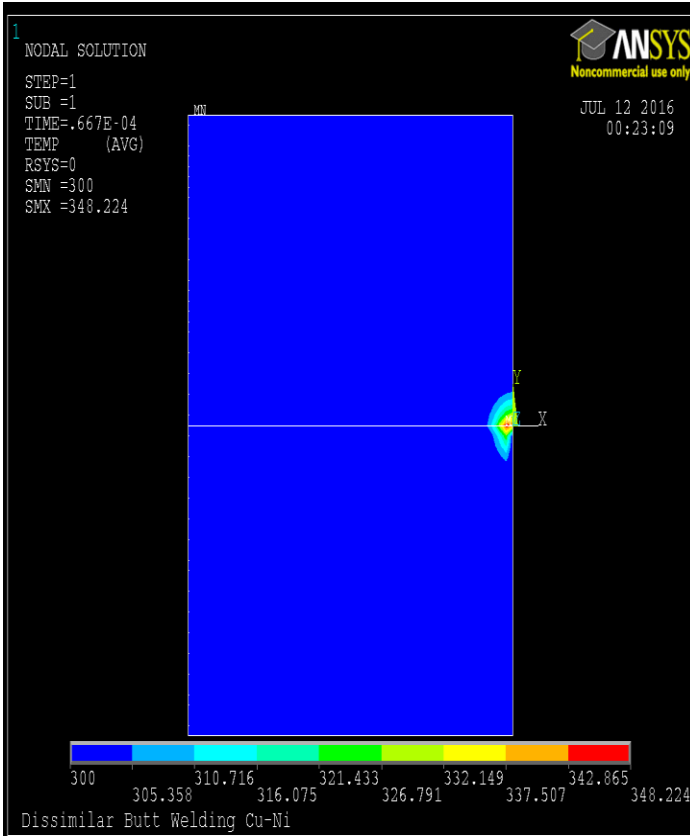
Figure. 4.14 Plot between the maximum temperatures reached in each of the load step versus the time

4.5 Average weld composition for dissimilar couple

In this section we showed the result of simulations of dissimilar couple of Cu/Ni and Ti/Ni. Each of the dimensions is divided in such a way that, each partition has a space of 0.2 mm. Processing parameters and base metals properties are mentioned in table 3.2, 3.3, 3.4.

4.5.1 Cu/Ni joint

We have shown the top view of weld met. Top plate is Cu and bottom plate is Ni. We can see the temperature contours in Fig. 4.15 with simulation details mentioned.



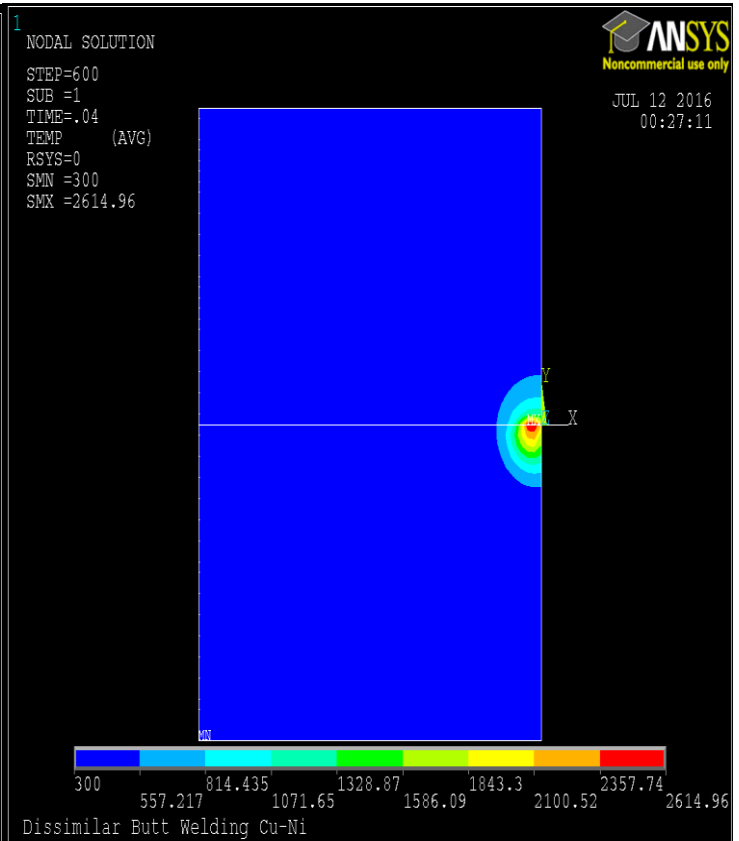
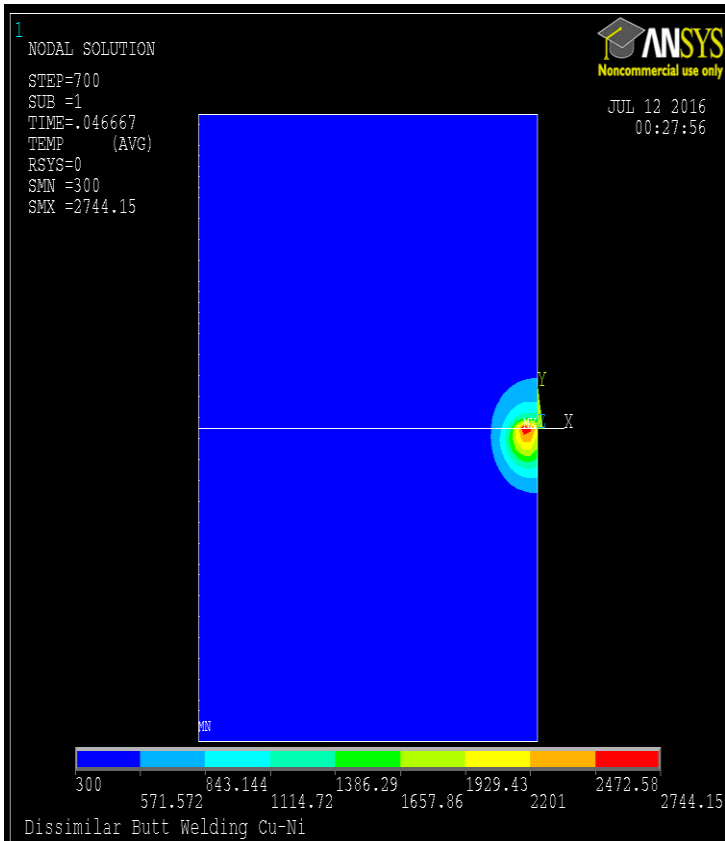
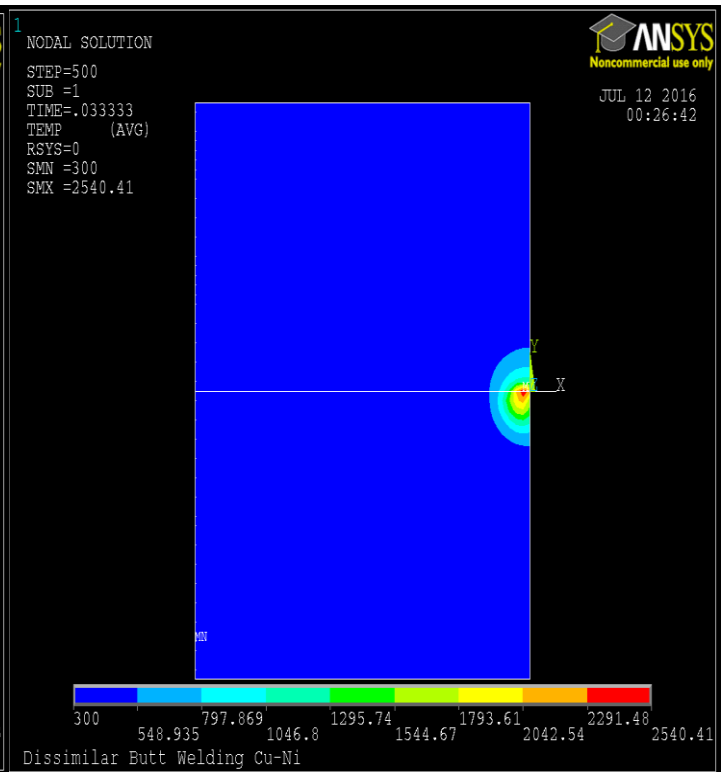
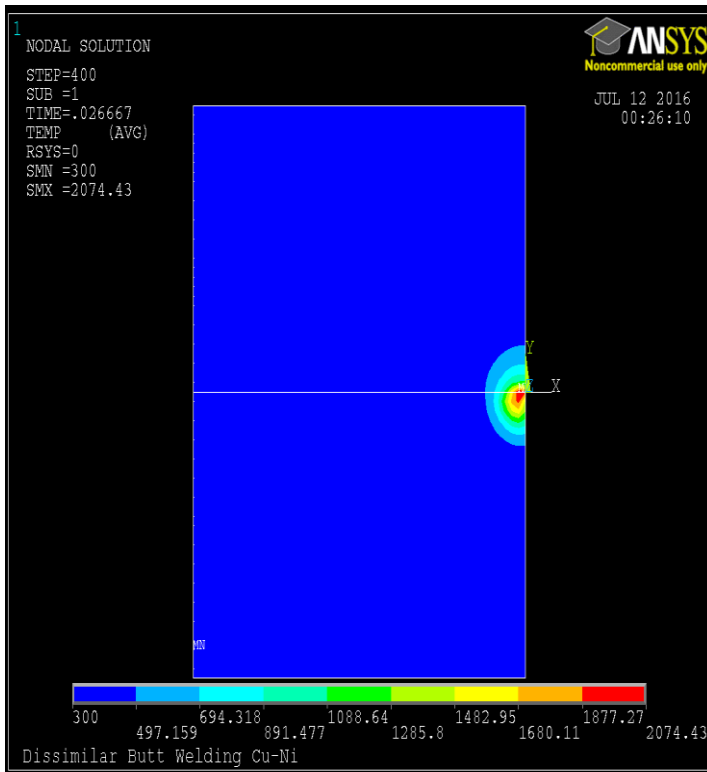


Figure. 4.15 (1, 2, 3 and 4) Evolution of temperature contours with time

Ni has lower thermal conductivity than Cu. This helps Ni to heat localize and melt more than Cu. Cu distributes the heat energy, which it received so it melt less than Cu. We can observe the maximum temperature concentrated on Ni side. Ni has melted more volume than Cu. The average composition found out to be Cu 30 at% - Ni for the given processing parameters

Chapter 5

Summary

We have studied the microstructural features of Ti/Ni joints. XRD, SEM and EDS have been used as characterizing tools to observe the microstructural features as well as composition at different locations in the weld pool of Ti/Ni.

Laser welding of Ti/Ni

Compositional, temperature gradients present during welding played a major role in deciding the microstructural features of the weld pool. The microstructural features include:

- Asymmetric weld pool is observed, which resulted Ti to melt more than Ni.
- Calculated average weld composition found to Ti-50 at% Ni.
- XRD results showed non-equilibrium solidification happened which resulted in presence of Ni_2Ti phase as well monoclinic and cubic TiNi to exist together.
- Ti_2Ni dendrites are growing towards Ti interface from the weld pool, which is in the direction of heat extraction.
- Three layers of IMCs observed parallel to Ni interface.
 - First layer is of (Ni) and faceted dendrites of Ni_3Ti .
 - Second layer is of $\text{Ni}_3\text{Ti}+\text{TiNi}$.
 - Third layer is of TiNi dendrites grown in all the directions.
- Middle of the weld pool is consist of TiNi dendrites and on top of weld pool TiN phase was observed because of not maintaining shielding gas.
- Macrosegregation of TiNi is observe at bottom of the weld pool.

These signifies the importance of fluid flow which decides the composition as well temperature gradients present during solidification, which finally effects the microstructural features.

Computational study

We have attempted to study the average weld pool composition variation with processing parameters by modelling analytical Rosenthal's 2D equation. Then we tried to model it by using FEM by using ANSYS. This has lead us to some interesting results:

- Rosenthal's analytical model revealed that with increasing heat input average weld composition varies.
 - A region of Ti rich to Ni rich is observed with increasing heat input in Ti/Ni binary couple
- Bench marking has done to written code, which solves heat conduction equation by FEM.
- The solution obtained is Oscillatory stable.
- Cu/Ni joint average weld composition is estimated for a given set of processing parameters.

References

1. Robert W. Messler: *Principles of Welding*
2. Sindo Kou: *Welding Metallurgy*
3. ASM Handbook (Volume 6): *Welding, Brazing and Soldering (ASM International, Metals Park, OH., 1993).*
4. T.W. Nelson, J.C. Lippold, M.J. Mills, “Nature and Evolution of the Fusion boundary in Ferritic-Austenitic Dissimilar weld metals”, *Welding Research Council*.
5. G. Phanikumar, P. Dutta, and K. Chattopadhyay: “Continuous welding of Cu–Ni dissimilar couple”. *Science and Technology of Welding and Joining*, 10 (2005), 158.
6. S. Chatterjee, T. A. Abinandanan, K. Chattopadhyay: “Microstructure development during dissimilar welding: Case of laser welding of Ti with Ni involving intermetallic phase formation”, *J Mater Sci* 41 (2006) 643–652.
7. A. Seretsky and B. Ryba: “Laser welding of dissimilar metals: Titanium to Nickel”. *Welding Journal*, 55 (1976), 208s.
8. Hui-Chi Chen , Andrew J. Pinkerton , Lin Li: “Fibre laser welding of dissimilar alloys of Ti-6Al-4V and Inconel 718 for aerospace applications” , *Int J Adv Manuf Technol*.
9. Shuhai Chen, Liqun Li, Yanbin Chen, Jihua Huang: “Joining mechanism of Ti/Al dissimilar alloys during laser welding-brazing process”, *Journal of Alloys and Compounds* 509 (2011) 891–898
10. R. Cao, Z. Feng, J.H. Chen: “Microstructures and properties of titanium–copper lap welded joints by cold metal transfer technology”, *Materials and Design* 53 (2014) 192–201
11. Kemal Aydın, Yakup Kaya, Nizamettin Kahraman: “Experimental study of diffusion welding/bonding of titanium to copper”, *Materials and Design* 37 (2012) 356–368
12. Liu Jia , Jiang Shichun, Shi Yan, Ni Cong, Chen junke, Huang Genzhe: “Effects of zinc on the laser welding of an aluminum alloy and galvanized steel”, [Journal of Materials Processing Technology Volume 224](#), October 2015, Pages 49–59
13. P. Xue, B.L. Xiao, D.R. Ni, Z.Y. Ma, “Enhanced mechanical properties of friction stir welded dissimilar Al-Cu by intermetallic compound formation”, *Materials Science and Engineering, Volume 527*, 5723-5727.

14. B. Majumdar, R. Galun, A. Weisbejt, B. L. Mordike: "Formation of a crack-free joint between Ti alloy and Al alloy by using a high-power CO₂ laser", *Journal of Materials Science* 32 (1997) 6191–6200
15. Liming Liu, Daxin Ren and Fei Liu, "A Review of Dissimilar Welding Techniques for Magnesium Alloys to Aluminum Alloys", *Materials* 2014, 7, 3735-3757
16. T.A. Mai, A.C. Spowage: "Characterisation of dissimilar joints in laser welding of steel–kovar, copper–steel and copper–aluminium", *Materials Science and Engineering A* 374 (2004) 224–233.
17. Z.Sun, J.C.Ion, " Review laser welding of dissimilar metal combinations", *Journal Materials Science* 30 (1995) 4205-4214.
18. Metzger and R.Lison, "Electron beam welding of dissimilar metals", *Welding Journal*, 55 (1976), 230s.
19. J. Mazumdar, " Advantages of laser welding over other welding processes", *J. Metals* 34 (1982) 16
20. Apurv Choubey, Vijay Kumar: "Influence of Heat Input on Mechanical Properties and Microstructure of Austenitic 202 grade Stainless Steel Weldment", *WSEAS Transactions on Applied and Theoretical Mechanics*.
21. Chen Guo-qing, Zhang Bing-gang, Liu Wei, Feng Ji-cai, "Influence of electron-beam superposition welding on intermetallic layer of Cu/Ti joint", *Trans. Nonferrous Met. Soc. China* 22(2012) 24162420
22. John Goldak, Aditya Chakravarti, and Malcolm Bibby, "A New Finite Element Model for Welding Heat Sources", *Metallurgical Transactions B Volume 15B*, June 1984-- 301
23. Gandham Phanikumar, Sambanadam Manjini, Pradip Dutta, Jyotirmoy Mazumder, and Kamino Chattopadhyay: "Characterization of a Continuous CO₂ Laser–Welded Fe-Cu Dissimilar Couple", *Metallurgical and Materials Transactions A Volume 36A*, August 2005—2147
24. Hongtao Zhang, Peng He, Jicai Feng, Huiqiang Wu: "Interfacial microstructure and strength of the dissimilar joint Ti3Al/TC4 welded by the electron beam process ", *Materials Science and Engineering A* 425 (2006) 255–259.
25. Yanbin Chen, Shuhai Chen, Liqun Li: Effects of heat input on microstructure and mechanical property of Al/Ti joints by rectangular spot laser welding-brazing method", *Int J Adv Manuf Technol* (2009) 44:265–272.

26. Chengwu Yao, BinshiXu, XianchengZhang, JianHuang, JunFu, YixiongWu: “Interface microstructure and mechanical properties of laser welding copper–steel dissimilar joint”, *Optics and Lasers in Engineering* 47 (2009) 807–814.
27. Shusen Zhao, Gang Yub, Xiuli Heb, Yaowu Hub: “Microstructural and mechanical characteristics of laser welding of Ti6Al4V and lead metal”, *Journal of Materials Processing Technology* 212 (2012) 1520– 1527.
28. Schubert E, Klassen M, Zerner: “Light-weight structures produced by laser beam joining for future applications in automobile and aerospace industry”, *J Mater Process Technol* 115:2–8
29. Subhradeep Chatterjee, T. A. Abinandanan, G. Madhusudhan Reddy, Kamanio Chattopadhyay, “ Microstructure Formation in Dissimilar Metal Welds: Electron Beam Welding of Ti/Ni “
30. Buehler, W. J.; Gilfrich, J. W.; Wiley, R. C. (1963). "Effects of Low-Temperature Phase Changes on the Mechanical Properties of Alloys Near Composition TiNi". *Journal of Applied Physics* 34 (5): 1475–1477
31. Wang, F. E.; Buehler, W. J.; Pickart, S. J. (1965). "Crystal Structure and a Unique Martensitic Transition of TiNi". *Journal of Applied Physics* 36 (10): 3232–3239.
32. S. Chatterjee, T.A. Abinandanan, K. Chattopadhyay, “Phase-Field Simulation of Fusion Interface Events during Solidification of Dissimilar Welds: Effect of Composition Inhomogeneity”, *The Minerals, Metals & Materials Society and ASM International* 2007
33. P. S. Liu, W. A. Baeslack, and J. Hurley: “Dissimilar alloy laser beam welding of titanium: Ti–6Al–4V to β -C”. *Welding Journal*, 73 (1994), 175s.
34. W.F. Gale & T.C Totomeir: *Smithells Metals Reference Book*
35. Edward H. Kottcamp, Edward L. Langer : *Handbook of Alloy Phase Diagrams* (ASM International, 1992).